JOURNAL OF PETROLOGY | VOLUME 43 | NUMBER 8 | PAGES 1469–1503 | 2002

The Fish Canyon Magma Body, San Juan Volcanic Field, Colorado: Rejuvenation and Eruption of an Upper-Crustal Batholith

OLIVIER BACHMANN[1]*, MICHAEL A. DUNGAN[1] AND PETER W. LIPMAN[2]

[1]SECTION DES SCIENCES DE LA TERRE DE L'UNIVERSITÉ DE GENÈVE, 13, RUE DES MARAÎCHERS, 1211 GENEVA 4, SWITZERLAND

[2]US GEOLOGICAL SURVEY, 345 MIDDLEFIELD ROAD, MENLO PARK, CA 94025, USA

RECEIVED MAY 11, 2001; REVISED TYPESCRIPT ACCEPTED JANUARY 22, 2002

More than 5000 km^3 of nearly compositionally homogeneous crystal-rich dacite (~68 wt % SiO_2: ~45% Pl + Kfs + Qtz + Hbl + Bt + Spn + Mag + Ilm + Ap + Zrn + Po) erupted from the Fish Canyon magma body during three phases: (1) the pre-caldera Pagosa Peak Dacite (an unusual poorly fragmented pyroclastic deposit, ~200 km^3); (2) the syn-collapse Fish Canyon Tuff (one of the largest known ignimbrites, ~5000 km^3); (3) the post-collapse Nutras Creek Dacite (a volumetrically minor lava). The late evolution of the Fish Canyon magma is characterized by rejuvenation of a near-solidus upper-crustal intrusive body (mainly crystal mush) of batholithic dimensions. The necessary thermal input was supplied by a shallow intrusion of more mafic magma represented at the surface by sparse andesitic enclaves in late-erupted Fish Canyon Tuff and by the post-caldera Huerto Andesite. The solidified margins of this intrusion are represented by holocrystalline xenoliths with Fish Canyon mineralogy and mineral chemistry and widely dispersed partially remelted polymineralic aggregates, but dehydration melting was not an important mechanism in the rejuvenation of the Fish Canyon magma. Underlying mafic magma may have evolved H_2O–F–S–Cl-rich fluids that fluxed melting in the overlying crystal mush. Manifestations of the late up-temperature magma evolution are: (1) resorbed quartz, as well as feldspars displaying a wide spectrum of textures indicative of both resorption and growth, including Rapakivi textures and reverse growth zoning ($An_{27–28}$ to $An_{32–33}$) at the margins of many plagioclase phenocrysts; (2) high Sr, Ba, and Eu contents in the high-SiO_2 rhyolite matrix glass, which are inconsistent with extreme fractional crystallization of feldspar; (3) oscillatory and reverse growth zoning toward the margins of many euhedral hornblende phenocrysts (rimward increases from ~5·5–6 to 7·7–8·5 wt % Al_2O_3). Homogeneity in magma composition at the chamber-wide scale, contrasting with extreme textural and chemical complexities at the centimeter–millimeter scale, is consistent with a dynamic environment, wherein crystals with a variety of growth and resorption histories were juxtaposed shortly before eruption by convective currents.

KEY WORDS: *Monotonous Intermediates; ignimbrite; silicic magmatism; magma rejuvenation*

INTRODUCTION

The Fish Canyon Tuff is the product of the largest documented pyroclastic eruption (Lipman *et al.*, 1970; Whitney & Stormer, 1985; Lipman, 2000) and the archetypal example of a group of voluminous silicic ignimbrites referred to by Hildreth (1981) as the 'Monotonous Intermediates'. These dominantly dacitic magmas are important for the understanding of crustal magmatism, not only because they are the largest known manifestations of explosive volcanism on Earth (a few hundreds of km^3 to >5000 km^3 for a single eruption), but also because such ash-flow sheets provide a link between the plutonic and volcanic realms. Indeed, they resemble erupted batholiths in the sense that they have comparable volumes, occur in the same tectonic settings, and are

*Corresponding author: Present address: University of Washington, Department of Earth and Space Sciences, Mailstop 351310, Seattle, WA 98195-1310, USA. Telephone: (206) 543 2827 (office). Fax (shared): (206) 543 3836. E-mail: bachmann@ess.washington.edu

© Oxford University Press 2002

characterized by high crystal contents (~40–50%), near-solidus mineral assemblages, and a lack of evidence for compositional zoning in pre-eruptive magma chambers (Francis *et al.*, 1989; de Silva, 1991).

Some of the most controversial issues in the study of silicic magmatism are the thermal evolution and residence times of large upper-crustal magma bodies and whether silicic magmas are generated dominantly by crystal fractionation or by melting of pre-existing crustal material. In particular, the question of residence time of magmas in the upper crust has been debated (see Halliday, 1990; Mahood, 1990; Sparks *et al.*, 1990; Reid *et al.*, 1997; Brown & Fletcher, 1999; Reid & Coath, 2000), following the inference, based on Rb–Sr and $^{40}Ar/^{39}Ar$ data from the Long Valley system (Halliday *et al.*, 1989; van den Bogaard & Schirnick, 1995), that upper-crustal silicic magma bodies may remain partly molten for periods >1 Myr. In acknowledgement of the difficulty of maintaining a large magma body near its liquidus in the upper crust for such a long period, an alternative model was proposed in which the magma chamber is episodically reheated, with periods of crystallization alternating with periods of partial remelting following new magma inputs; that is, 'defrosting' of a crystal mush (Mahood, 1990).

The present reinvestigation of the Fish Canyon magmatic system, which has been extensively studied in the past (Lipman *et al.*, 1970, 1997; Whitney & Stormer, 1985; Johnson & Rutherford, 1989*a*; Riciputi *et al.*, 1995), has led to a new model for its petrologic evolution. A rich catalog of previously unrecognized textural and geochemical features, which are well preserved in recently identified non-fragmented samples of Fish Canyon magma of the Pagosa Peak Dacite and Nutras Creek Dacite (Bachmann *et al.*, 2000), serve as the basis for inferring that the Fish Canyon magma body was remobilized following a voluminous injection of mafic magma, which reheated and partially remelted an upper-crustal near-solidus crystal mush of batholithic dimensions. Similar models have been proposed for the Kos Ignimbrite (Keller, 1970), the Long Valley system (Mahood, 1990), and the southwest moat rhyolites of the Valles Caldera (Wolff & Gardner, 1995), as well as the continuing Soufrière Hills eruption on Montserrat (Murphy *et al.*, 2000; Couch *et al.*, 2001). The fact that these rhyolitic to andesitic eruptive products, with vastly different volumes, seem to have originated by the same mechanism may indicate that thermal rejuvenation of near-solidus upper-crustal intrusions shortly before eruption is a fairly common process in silicic systems. Moreover, this model does not require long upper-crustal residence times for largely molten magma bodies.

GEOLOGICAL SETTING

The San Juan volcanic field, located on the eastern margin of the Colorado plateau in SW Colorado, covers an area of ~25 000 km^2 with a total volume of ~40 000 km^3 of intermediate to silicic volcanic rocks. The San Juan volcanic field is the largest erosional remnant of a nearly continuous igneous province that extended over much of the southern Rocky Mountains during mid-Tertiary time (Steven, 1975). It lies at the northern tip of a succession of Tertiary volcanic fields extending south to the Sierra Madre Occidental, in present-day Mexico (Fig. 1). Although magmatic activity in the Sierra Madre Occidental is plausibly related to Oligocene subduction of the Pacific plate beneath North America, the tectonic setting of the volcanic fields that are located further to the north, several hundreds of kilometers inboard from the plate margin, is more controversial. The arc-like geochemical signature of San Juan magmas (e.g. high-K calc-alkaline series with high La/Nb and Ba/La) has led to the interpretation that low-angle subduction was associated with this magmatic activity (Lipman *et al.*, 1972, 1978), but magma generation from lithospheric mantle previously modified by subduction has been proposed as an alternative (Davis *et al.*, 1993).

Tertiary activity in the San Juan volcanic field began with a period of >4 Myr of andesitic magmatism (~33·5–29·5 Ma) in the form of large stratovolcanoes (Lipman *et al.*, 1970), which accumulated to thicknesses of 1–2 km across the entire area of the volcanic field. Voluminous explosive eruptions began before 29 Ma, and at least 17 large silicic ash-flow sheets (100–5000 km^3) and related post-collapse lavas were erupted during ~3 Myr from three nested caldera clusters in the west, central, and SE part of the field (Fig. 2; Steven & Lipman, 1976). Caldera-forming activity started in the west and SE caldera clusters and then converged on the central part of the field at ~28·5 Ma. The Fish Canyon magmatic system belongs to a sequence of nine major ash-flow tuffs and related lavas erupted during ~2·5 Myr (28·5–26 Ma) from the extremely productive central San Juan cluster, reaching a magma production rate of >4000 km^3/Myr (Lipman *et al.*, 1996). Andesitic activity was prevalent between caldera-related eruptions, as intermediate composition lavas and clast-rich laharic breccias are interlayered with the ignimbrites. San Juan magmatism ended with a Mio-Pliocene bimodal suite, the Hinsdale Formation, which was associated with crustal extension of the Rio Grande Rift (Lipman *et al.*, 1970, 1978).

The changes in eruptive style and chemical composition recorded by the products of the San Juan volcanic field reflect progressive crustal hybridization and emplacement of a composite high-level batholith during long-term intracontinental magmatism (Riciputi *et al.*, 1995). During the early stages, the eruptive products consisted mainly of andesitic lava flows, produced by differentiation of

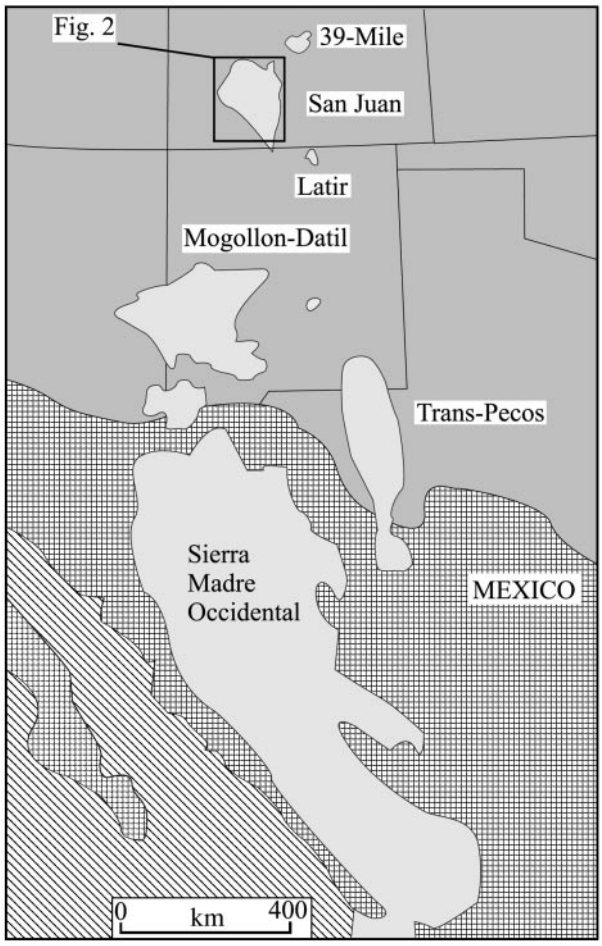

Fig. 1. Map of southwestern North America, emphasizing the alignment of mid-Tertiary volcanic fields extending from the apparently subduction-related magmatism of the Sierra Madre Occidental to the San Juan volcanic field, which is characterized by high-K calc-alkaline eruptive products with arc-like geochemical affinities, despite its unusually large distance from the western margin of the North American plate (>700 km). Modified from Davis *et al.* (1993).

mantle-derived basalts involving both fractional crystallization and crustal assimilation (Colucci *et al.*, 1991; Riciputi *et al.*, 1995). Volumetrically minor units with more evolved compositions appear in some sections, but basaltic magma apparently did not reach the surface during Oligocene magmatism. The relatively abrupt appearance of silicic ash-flow sheets at ~29–30 Ma, emplaced during large caldera-forming eruptions, marks the ascent of magma bodies to shallow levels and increased chemical contributions from the upper crust after several millions of years of crustal heating by injection of mantle-derived magmas. During the period dominated by explosive silicic volcanism, mantle input continued, as indicated by the andesitic units interlayered with the ignimbrites. This led to progressive hybridization of the crustal column within the main zone of magma transport and injection (Lipman *et al.*, 1978; Riciputi *et al.*, 1995). This long-term progression toward more evolved magma compositions and shallower magma storage has been interpreted as representing the emplacement and differentiation of a large composite batholith in the upper crust. This interpretation is corroborated by the presence of a large negative Bouguer gravity anomaly (down to −330 mgal) in the San Juan region (Plouff & Pakiser, 1972).

Recently, the eruptive history of the Fish Canyon magmatic system has been shown to be more complex than previously thought. The Fish Canyon magma chamber produced three separate but compositionally identical units with different eruptive styles in rapid succession ~28 Myr ago (Lipman *et al.*, 1997; Bachmann *et al.*, 2000). The Fish Canyon Tuff, with a total volume of ~5000 km^3, was erupted during the collapse of the ~100 km × 35 km La Garita caldera as a highly fragmented crystal-rich deposit containing only scarce small pumices. In contrast, the precursory Pagosa Peak Dacite eruption produced ~200 km^3 of poorly fragmented pyroclastic deposits, which are preserved around the southeastern edge of the La Garita caldera (Fig. 2). This unit, which was first recognized as a separate eruptive phase in 1995, and which is interpreted as the product of a low-energy fire-fountain eruption (Bachmann *et al.*, 2000), contains large low-vesicularity pumices, up to 4 m in diameter, referred to as magma 'blobs'. Unlike bulk Fish Canyon Tuff, the Pagosa Peak Dacite blobs closely approximate Fish Canyon magma compositions. Furthermore, they preserve magmatic textures, which have been largely destroyed in the Fish Canyon Tuff by shattering of phenocrysts (particularly feldspars) and dispersal of crystal fragments. The Nutras Creek Dacite is a small post-Fish Canyon lava flow (<1 km^3) on the north flank of the resurgent dome (Fig. 2), which has also yielded non-fragmented samples of Fish Canyon magma.

PREVIOUS INVESTIGATIONS OF THE FISH CANYON SYSTEM

The regional extent of the Fish Canyon Tuff, its large volume, distinctive petrologic character with respect to many ash-flow sheets (uniform dacitic composition, high phenocryst content, 11-phase mineral assemblage), and relation to large-scale caldera collapse were initially recognized more than 30 years ago (Lipman *et al.*, 1970; Lipman, 1975; Steven & Lipman, 1976). Hildreth (1981) called attention to the anomalous character of voluminous silicic units, which lack compositional zoning (Monotonous Intermediates), in light of the prevailing

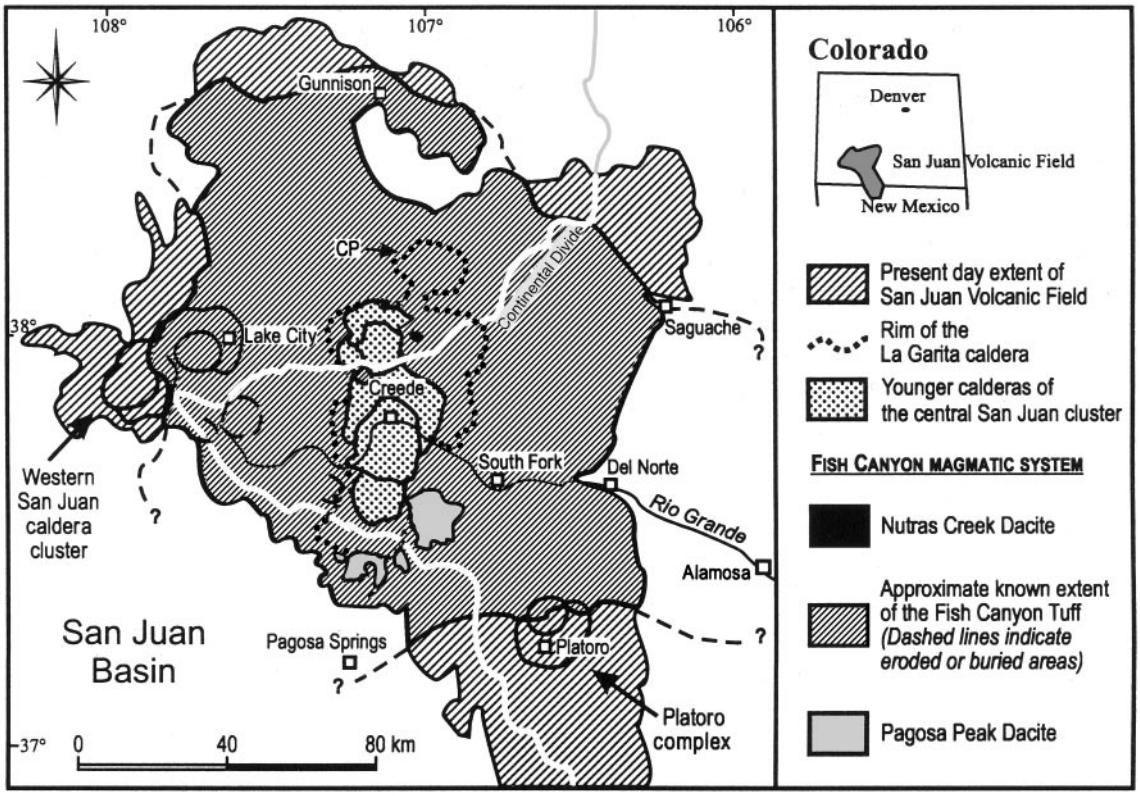

Fig. 2. Location map showing the preserved extent of the San Juan volcanic field and the approximate distribution of the outflow facies of the Fish Canyon Tuff (modified from Steven & Lipman, 1976). Ash-flow tuff volcanism in the San Juan volcanic field was concentrated in three caldera clusters. The source of the Fish Canyon eruptions is the La Garita caldera, the second (after buried source of Masonic Park Tuff) and largest of a series of eight calderas that form the central San Juan caldera cluster. The northernmost segment of the La Garita caldera was formerly referred to as the Cochetopa Park caldera (CP), but recent field work (by Lipman, in 1999–2000) has shown that this is a late, subsidiary collapse structure associated with the Fish Canyon Tuff eruption.

view that most such magmas were derived by differentiation from subjacent mafic parental magmas by crystal fractionation. Such an origin was, and still is, thought to produce chemical and thermal gradients or discontinuities in shallow magma chambers. However, erupted volumes of homogeneous silicic magma greater than a few thousand km^3 require extraordinarily large volumes of parental mafic magma. In effect, the question of how Monotonous Intermediate tuffs originate raises the same issues as does the origin of batholithic granitoid intrusions.

The pre-eruptive state of the Fish Canyon magma chamber was investigated by Stormer & Whitney (1985) and Whitney & Stormer (1985), who concluded that this chamber lacked compositional and thermal gradients and that the phenocrysts had equilibrated at 7–9 kbar before rapid ascent to shallow levels. Both conclusions were based on whole-rock and coexisting phase compositions in bulk samples of the Fish Canyon Tuff *sensu stricto*, which is notable for: (1) an extreme scarcity of pumices (fiamme) sufficiently large to permit direct determinations of magma composition; (2) shattering and dispersion of phenocrysts and glassy matrix during eruption and emplacement; (3) nearly pervasive devitrification of the matrix. Following criticism of these conclusions by Grunder & Boden (1987), Johnson & Rutherford (1989*a*, 1989*b*) used Fish Canyon Tuff as a starting material to determine the P, T, X_{H_2O}, and f_{O_2} at which the phenocryst assemblage equilibrated with residual melt and to experimentally calibrate the Al-in-hornblende geobarometer (Hammarstrom & Zen, 1986). Both methods yielded a pressure of $\sim 2{\cdot}4 \pm 0{\cdot}5$ kbar, strengthening arguments for upper-crustal residence and low-pressure equilibration of the Fish Canyon mineral assemblage, in accord with caldera collapse.

The large, easily extracted blobs of Fish Canyon magma in the Pagosa Peak Dacite and the recognition of the effusive origin of the Nutras Creek Dacite (Bachmann *et al.*, 2000) provide samples of unmodified magma composition, which have allowed us to test the assertion that the pre-eruptive Fish Canyon magma chamber lacked thermal and chemical gradients (Whitney & Stormer, 1985). These samples preserve textural information critical to the formulation of our new model for the genesis and evolution of the Fish Canyon magma

body. Because crystals were less broken during the relatively low-energy eruptions, numerous textural relationships that were not previously appreciated are evident (see Figs 10, 12, 13 and 15–18, below). In particular, resorption textures are not limited to quartz, but also are widespread in feldspar phenocrysts, and evidence of grain boundary melting is preserved when the two feldspar phases or feldspars and quartz are in contact (see Figs 12, 17 and 18, below).

MODAL ABUNDANCES

The Fish Canyon magma is a crystal-rich (40–45% crystals) dacite characterized by a low-variance mineral assemblage, consisting of two feldspars, quartz, hornblende, biotite, Fe–Ti oxides, apatite, sphene, zircon, and rare pyrrhotite, in a microlite-free interstitial melt of high-silica rhyolite (76·7–77·7 wt % SiO_2, recalculated to 100% anhydrous, as are all major element compositions reported in the text of this paper). These attributes characterize all three stratigraphic units that make up the Fish Canyon magmatic system. Modal abundances of phenocrysts are similar among Pagosa Peak Dacite blobs and Nutras Creek Dacite samples. Phenocryst abundances in these samples of non-fragmented Fish Canyon magma are generally lower than in the Fish Canyon Tuff (Table 1). The coarse grain size of some phases (up to 5 mm), the heterogeneous distribution of minerals on the centimeter scale, and uncertainties in distinguishing quartz and sanidine in thin section all impede highly accurate modal counting. Variations in measured modal feldspars, quartz, and hornblende among Pagosa Peak Dacite samples (Table 1) probably reflect the difficulty of obtaining accurate estimates as much as real variability. Despite these obstacles, the impact of glass winnowing during ash-flow emplacement is perceptible (Table 1). One outflow Fish Canyon Tuff sample ('Elep') is ~11% more crystal rich than any magma blob from the Pagosa Peak Dacite.

Table 1: Modal analyses of samples from different units of the Fish Canyon magmatic system

Sample:	Bfc 59	Bfc 83	Bfc 13	Bfc 12	Bfc 115	Average
Unit:	PPD	PPD	PPD	PPD	NCD	PPD+NCD
Plagioclase	28·1	23·9	26·4	26·0	26·6	26·2
K-feldspar	5·7	9·6	4·3	4·3	6·5	6·1
Quartz	3·9	4·3	1·2	2·2	3·6	3·0
Hornblende	1·8	3·7	6·8	4·3	2·4	3·8
Biotite	3·4	2·8	5·3	3·5	3·2	3·6
Sphene	0·2	0·2	0·3	1·3	1·3	0·7
Opaques	0·0	0·7	1·3	0·2	0·1	0·5
Matrix	57·0	54·9	54·4	58·2	56·3	56·2
% pheno.	43·0	45·1	45·6	41·8	43·7	43·8

Sample:	Bfc 49	Elep	Range	Bfc 134	Bfc 187	CsGr10
Unit:	FCT	FCT	W&S (1985)*	Gran. xeno.	Gran. xeno.	Gran. xeno.
Plagioclase	26·8	31·4	20–30	32·4	34·7	~40
K-feldspar	4·7	7·5	6–13	30·8	28·8	~25
Quartz	3·7	4·7	1–8	21·9	24·6	~25
Hornblende	3·2	4·5	1–4·5	3·5	3·8	4·4
Biotite	3·6	4·8	2·5–7	8·4	5·0	3·7
Sphene	0·3	0·7	0·1–0·5	0·5	0·7	0·5
Opaques	1·4	1·3	1–3	2·6	2·4	1·4
Matrix	56·3	45·4	50–60	—	—	—
% pheno.	43·7	54·6	40–50	—	—	—

Representative modal data for the Fish Canyon magmatic system. Measurements for the Fish Canyon magma were obtained from Pagosa Peak Dacite blobs and Nutras Creek Dacite, to avoid biased results caused by crystal–ash fractionation. Total number of points was 2000/section. Abundances of sanidine and quartz in xenoliths are relatively inaccurate because of similar appearance in thin sections. PPD, Pagosa Peak Dacite; FCT, Fish Canyon Tuff; NCD, Nutras Creek Dacite; Gran. xeno., granodioritic xenolith. CsGr10 contains interstitial granophyre.
*Measurements of Whitney & Stormer (1985) were performed uniquely on Fish Canyon Tuff samples (Agua Ramon section, Goodrich Creek section, Beaver Creek section).

WHOLE-ROCK CHEMISTRY

Whitney & Stormer (1985) reported whole-rock major element compositions for Fish Canyon Tuff (outflow tuff facies from the region SSE of the La Garita caldera) ranging in SiO_2 wt % from ~62·5 to 67·5. On the basis of mass-balance calculations tied to glass compositions and crystal contents, they concluded that the Fish Canyon magma is a high-SiO_2 dacite (quartz latite in their nomenclature) with ~67–68 wt % SiO_2, and that the compositions with lower SiO_2 are the products of variable syn-eruptive crystal–ash fractionation (glass elutriation). We have analyzed 17 bulk Fish Canyon Tuff samples (16 outflow and one intracaldera) with widespread geographic coverage, including one with an extremely high crystal content (~55%; Elep, Table 2). Our data range from 65·4 to 68·5 wt % SiO_2, so we have not been able to reproduce the wide spectrum of SiO_2 values reported by Whitney & Stormer (1985). For most major elements (Fig. 3), our Fish Canyon samples define linear correlations with SiO_2 [compare with fig. 3 of Whitney & Stormer (1985)], and these data fall on trends extrapolated

from glass compositions (electron microprobe analyses) and the average composition of Pagosa Peak Dacite magma blobs [compare samples 1, 83, 55 and 34, Table 2 and analysis 10, table 6 of Lipman (1975)], which we infer to be representative of bulk magma compositions. The three least crystal-rich tuff samples fall close in major element composition to the average Pagosa Peak Dacite, as do a large fiamme from the northern intracaldera facies of the Fish Canyon Tuff (sample 129, Table 2) and the post-collapse Nutras Creek Dacite (sample 115, Table 2).

On the basis of these data, we infer that the major element range of Fish Canyon magma compositions was narrowly restricted (~67·5–68·5 wt % SiO_2), but not homogeneous within the limits of analytical precision. As both early-erupted and late-erupted magma compositions are similar, and there are few systematic variations in mineral chemistry among the eruptive phases, our data confirm the inference that the Fish Canyon magma chamber was not characterized by strong compositional and thermal gradients (large variations in Cl are due to degree of devitrification). Small, fine-grained mafic magmatic inclusions are found in the late-erupted intracaldera facies of the northern collapse depression (QMI 2, Table 2; see the section 'Magmatic inclusions'). Although these inclusions are hybridized (mixing with Fish Canyon magma), the linear trends defined by glass and whole-rock compositions of Fish Canyon material do not project toward the analyzed inclusion for most elements (Fig. 3). This observation is in accord with the virtual absence of quenched fragments of andesitic magma in more than 250 Fish Canyon samples that we have examined.

Variations of some trace elements in non-fragmented samples (i.e. magmatic compositions) span wider ranges than do major elements in the same samples. Although the Nutras Creek Dacite and pumice from the intracaldera Fish Canyon Tuff are indistinguishable from the average Pagosa Peak Dacite blobs in terms of almost all trace elements (Ba alone is low in pumice), there are differences among Pagosa Peak Dacite blob samples of the order of 15% relative for Y and heavy rare earth elements (HREE) (La/Yb ~18–21) and 10% for Zr and Hf. Given the presence of multiple accessory phases (apatite, zircon, sphene), it is difficult to assess the role of modal differences among analyzed splits of material vs first-order magmatic processes in generating these variations.

On the basis of the linear arrays defined by the Fish Canyon Tuff samples and glass in major element variation diagrams (Fig. 3) and the elemental enrichments and depletions illustrated in Fig. 4, we concur with Whitney & Stormer (1985) that most of the compositional variability among Fish Canyon Tuff samples is likely to be the result of syn-eruptive crystal–ash fractionation, not the presence of substantial pre-eruptive compositional gradients in the magma chamber. In addition, although there are previously unrecognized quenched andesite inclusions in the intracaldera facies, volumetrically important mingling or mixing with a more mafic component does not appear to be a factor in generating even the small observed variability. In light of the probability that the magma chamber was weakly heterogeneous, such heterogeneities do not appear to have been erupted in a systematic fashion, with the possible exception of the preferential occurrence of andesitic inclusions in late-erupted intracaldera tuff. We emphasize that the sampling of multiple eruptive phases of the Fish Canyon magmatic system in this study provides a more solid basis than previous datasets for documenting variations in magma composition and interpreting them.

As noted by Whitney & Stormer (1985), the Fish Canyon magma is similar for most major elements to average granodiorite (Nockolds *et al.*, 1978). Moreover, the products of the Fish Canyon magmatic system closely approximate the average composition of the upper continental crust proposed by Taylor & McLennan (1985; Fig. 5). In comparison with the latter, the Fish Canyon magma is higher in Ba, Th, K_2O (and total alkalis), and light REE (LREE) in accord with the relatively high-K nature of San Juan volcanism. The Fish Canyon magma is also notable in having a more pronounced negative Nb–Ta anomaly, and therefore an apparent arc-like signature (Ba/Nb ~50 vs 22 for the crust; La/Nb ~2·5 vs 1·2), but we emphasize that the Fish Canyon composition has relatively high Nb and Ta (16–18 ppm Nb and 1·1–1·2 ppm Ta) in comparison with dacitic magmas from modern continental margin arcs. We concur with Whitney & Stormer (1985) that the similarity of the Fish Canyon magma to average granodiorite (and average upper crust) implies that the processes involved in the generation of the Fish Canyon magma were similar to those that are typically responsible for the generation of batholithic intrusions.

PHENOCRYST TEXTURES AND CHEMISTRY

Our re-examination of phenocryst textures and compositions in the Fish Canyon magma has revealed greater textural variability in feldspars, and greater compositional variability in feldspars and ferromagnesian phases than previously reported by Whitney & Stormer (1985) and Johnson & Rutherford (1989*a*). The following sections discuss each phase separately, and first-order interpretations of the observed chemical variations are provided, before these results are integrated in a petrologic model.

Table 2: Whole-rock analyses of representative samples from the Fish Canyon magmatic system

Label:	1	83	55	34	124	49	Elep	129	115	QMI 2	CsGr 16	±2σ
Descr.:	PPD	PPD	PPD	PPD	FCT vitr. (O)	FCT (O)	FCT (O)	FCT pum (I)	NCD	Hybr. inc.	Gran. xeno	
SiO_2	68·79	68·26	68·51	68·49	67·47	68·00	65·37	67·82	67·93	57·92	67·16	<0·2
TiO_2	0·44	0·44	0·41	0·45	0·46	0·45	0·58	0·47	0·49	1·01	0·38	<0·05
Al_2O_3	15·16	15·38	15·48	15·23	15·89	15·63	16·32	15·25	15·23	16·55	14·30	<0·1
Fe_2O_3	3·40	3·55	3·45	3·49	3·73	3·70	4·85	3·97	4·14	7·44	3·05	<0·1
MnO	0·07	0·09	0·08	0·07	0·08	0·07	0·11	0·10	0·10	0·16	0·19	<0·01
MgO	0·98	0·92	0·93	0·80	0·92	0·93	1·13	1·23	0·85	2·94	0·84	<0·1
CaO	2·83	2·91	2·92	2·73	3·06	2·98	3·47	3·05	2·79	5·84	4·31	<0·1
Na_2O	3·70	3·92	3·9	3·89	3·91	3·78	3·85	3·79	3·66	3·29	3·53	<0·1
K_2O	4·19	4·35	4·12	4·29	4·10	4·10	4·15	3·94	4·42	3·42	4·37	<0·05
P_2O_5	0·18	0·18	0·18	0·19	0·18	0·19	0·24	0·20	0·20	0·42	0·17	<0·01
Total	99·73	99·99	99·98	99·63	99·80	99·83	100·06	99·82	99·81	99·78	100·17	
mg-no.	0·36	0·34	0·35	0·31	0·33	0·33	0·32	0·38	0·29	0·28	0·22	
LOI	0·21	1·72	0·34	0·37	0·90	0·88	0·40	0·70	0·94	0·77	1·88	
Ni	6·1	5·3	5·8	5·7	5·9	6·8	6·7	5·7	6·8	25·0		<0·5
Cr	5	8	5	7	5	7	7	5	6	58	4	<1
Co	5·4	6·1	7·4	6·3	6·5	7·5	9·2	7·1	7·1	19·3		<1
V	48·4	48·9	44·2	39·0	52·5	53·3	64·7	51·3	56·3	150·0	42·0	<5
Sc	5·3	6·6	6·0	5·9	6·3	6·5	8·1	6·57	6·0	16·5		<1
Cu	7·1	8·3	7·4	8·3	10·0	8·3	12·4	10·6	10·9			<1
Zn	46	92	67	50	58	58	68	56	64	100	34	<5
Cl	242	657	336	63	235	249	44	102	218			<50
Ga	16·8	17·6	18·5	18·3	17·6	17·6	18·8	17·8	18·2	22·0	17·0	<1
Pb	15·9	17·3	17·4	16·5	16·6	18·3	13·1	17·1	17·1	12·0	11·0	<1
Sr	438	439	454	431	487	453	570	456	436	839	384	<5
Rb	116·8	119·8	112·2	119·1	109·6	114·7	96·0	117·2	122·8	98·0	123·4	<5
Ba	865	835	880	839	891	810	1035	638	849	1275	933	<10
Zr	182	187	172	186	174	181	195	180	192	208	172	<10
Nb	17·8	17·1	15·5	16·6	16·0	16·6	15·9	16·9	17·3	13·2		<1
Th	13·9	13·6	13·8	14·1	12·4	13·2	9·8	13·8	12·9	5·8	11·0	<1
U	5·6	6·0	5·1	4·0	3·9	4·4	2·3	4·3	4·5	2·1		<1
Y	21·4	22·1	18·9	19·5	21·9	23·8	24·5	21·4	26·4	21·2	19·5	<1
Ta	1·2	1·2	1·1	1·2	1·1	1·1	1·0	1·1	1·1	0·7		<0·1
Hf	4·9	5·4	4·9	5·3	4·7	5·1	5·3	5·0	5·0	5·2		<0·5
Cs	3·2	2·9	2·9	2·5	2·4	2·4	1·0	2·4	3·3	1·7		<0·5
La	43·7	43·3	42·6	42·8	40·2	45·0	40·6	43·6	45·4	41·9	41·0	<1
Ce	85·3	84·8	81·5	82·8	81·0	86·0	83·0	82·0	81·1	84·7	75·0	<1
Nd	33·8	33·4	30·2	32·5	31·5	32·9	35·6	31·1	32·1	39·8	15·6	<1
Sm	5·73	5·75	5·24	5·42	5·42	5·91	6·29	5·40	5·44	7·59		<0·5
Eu	1·16	1·22	1·10	1·15	1·24	1·24	1·46	1·17	1·22	1·87		<0·5
Tb	0·62	0·64	0·54	0·56	0·63	0·68	0·70	0·65	0·67	0·79		<0·1
Yb	2·38	2·39	2·07	2·21	2·21	2·59	2·45	2·26	2·32	2·04		<0·5
Lu	0·37	0·36	0·32	0·33	0·34	0·41	0·37	0·33	0·36	0·33		<0·1

Major and trace elements on all samples, except CsGr16 and QMI 2, determined by XRF in University of London at Royal Holloway and Bedford New College (G. F. Marriner, M. F. Thirlwall, and O. Bachmann analysts). Samples CsGr16 and QMI were analyzed by XRF at the University of Lausanne (F. Capponi analyst). On samples 1, 83, 55, 34, 124, 49, ELEP, 115, and QMI 2, all the REE and Th, U, Ta, Hf, Cs, Zn, Co, Cr, and Sc were analyzed by INAA at the Open University (N. Rogers analyst). PPD, Pagosa Peak Dacite; FCT, Fish Canyon Tuff; NCD, Nutras Creek Dacite; I, intracaldera; O, outflow; Vitr., vitrophyre; Hybr. inc., hybrid andesite inclusion; Gran. xeno., granodioritic xenolith. Analytical errors (±2σ) estimated with reproducibility and analytical precision.

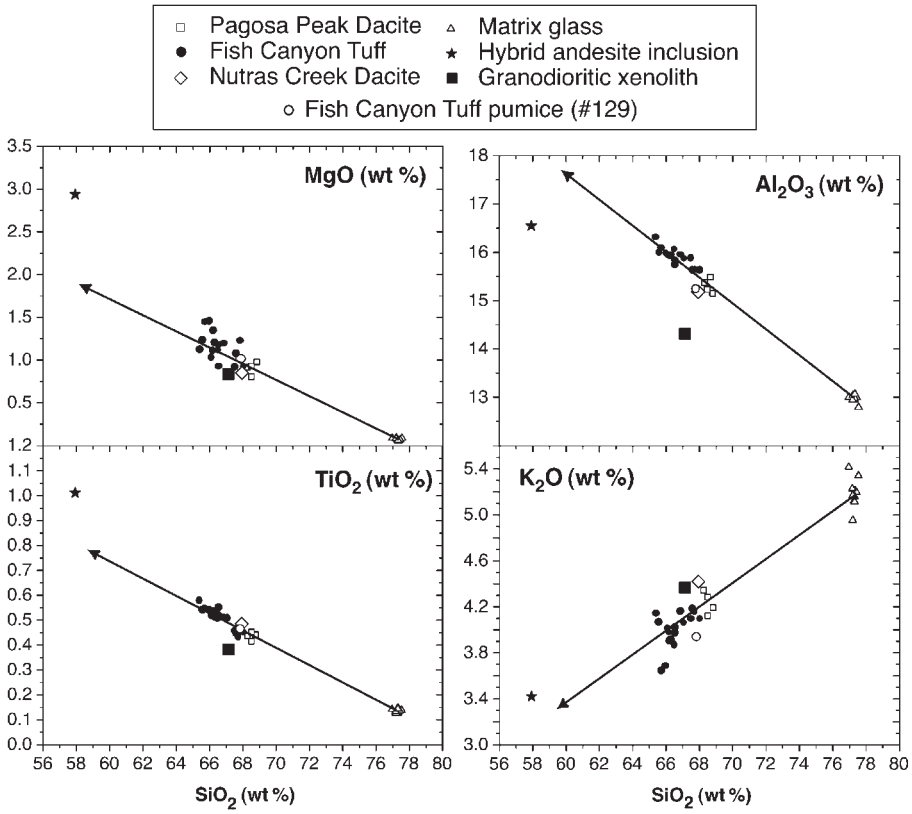

Fig. 3. Major element Harker variation diagrams for the Fish Canyon magmatic system (wt % oxides normalized to anhydrous values). The data plotted in these diagrams are those reported in Table 2 (Pagosa Peak Dacite, Nutras Creek Dacite and granodioritic xenolith) plus additional Fish Canyon Tuff samples for which we do not have the complete range of trace element data.

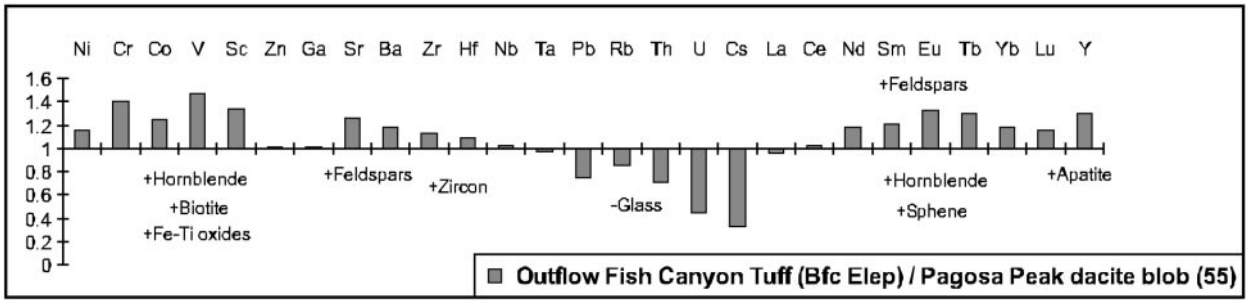

Fig. 4. Trace element enrichment–depletion diagram; the most crystal-rich Fish Canyon Tuff sample (Elep) is normalized to a Pagosa Peak Dacite blob sample (55), which is representative of non-fragmented Fish Canyon magma. This diagram illustrates general consequences of crystal–ash fractionation during pyroclastic flow transport and emplacement. Fine particles of ash are preferentially lost during transport, and tuff samples are enriched in crystals with respect to non-fragmented magma. Elements concentrated in one or more of the nine solid phases are enriched (>1) by as much as 30–40% relative to the magma composition, whereas those few elements that are incompatible with respect to all the mineral phases are depleted (<1) in the tuff.

Biotite

Biotite phenocrysts in Fish Canyon magma, 0·5–5 mm in size, are euhedral (Fig. 6) and have compositions typical of large dacitic crystal-rich ash-flow sheets, such as the Atana (Lindsay *et al.*, 2001) and Cerro Galan ignimbrites (Francis *et al.*, 1989). Grain-to-grain variations in major elements are up to 5 wt % absolute for FeO and MgO, but few inter-element correlations are apparent in the dataset as a whole, apart from slightly higher Fe/(Fe + Mg) in the intracaldera Fish Canyon Tuff and Nutras Creek Dacite (Table 3; Fig. 7). High-resolution (8–15 μm step), core-to-rim electron microprobe traverses across

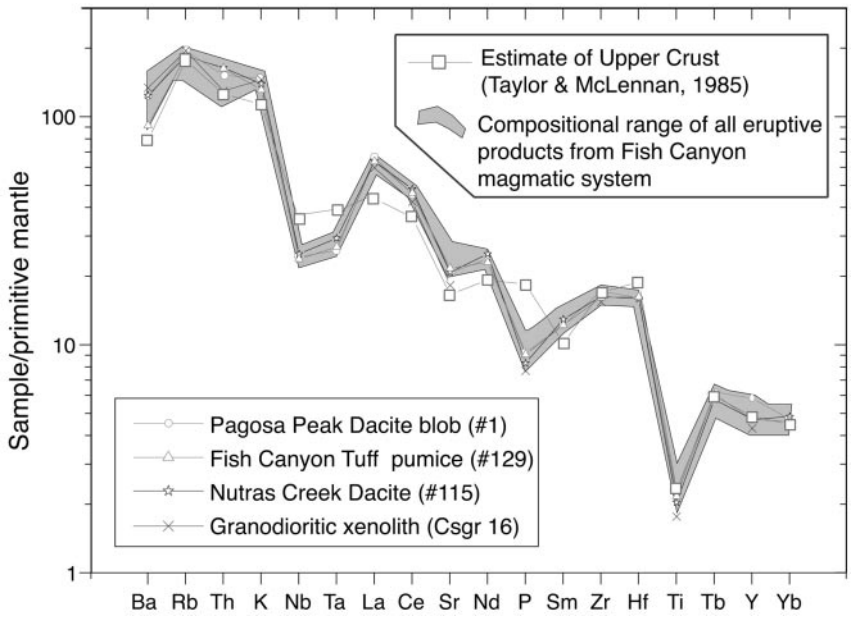

Fig. 5. Mantle-normalized multi-element diagram comparing the compositions of the eruptive products of the Fish Canyon magmatic system with (1) an estimate of the composition of the upper crust by Taylor & McLennan (1985), and (2) a granodioritic xenolith with Fish Canyon mineralogy and mineral chemistry (collected from intracaldera Fish Canyon Tuff). Concentrations are normalized to the primitive mantle composition of Sun & McDonough (1989). Representative non-fragmented samples from the Pagosa Peak Dacite, Fish Canyon Tuff, and Nutras Creek Dacite, as well as the analysis of the granodioritic xenolith, are plotted to illustrate the absence of large systematic differences between the early- and late-erupted products of the Fish Canyon magmatic system. The shaded field encompasses all the analyses listed in Table 2, and these account for the total variability of the Fish Canyon magma, as well as modifications caused by crystal–ash fractionation during transport (Figs 3 and 4).

biotite phenocrysts from all three stratigraphic units of the Fish Canyon system display nearly flat zoning profiles for major and minor elements, with the exception of fluorine, which varies from 0·8–0·9 wt % absolute to >2 wt %, both as relatively abrupt spikes in the internal parts of the crystals and as a progressive increase towards rims. Fluorine replacement of OH^- in micas depends primarily on: (1) the activity of HF in the melt during crystallization; (2) the temperature at which the F–OH exchange occurs; (3) the composition of the octahedral layer in the mica, in particular the Mg/Fe ratio (Munoz, 1984). As F variations in Fish Canyon biotites are largely independent of Mg/Fe, we suggest that temperature and/or the activity of HF in the melt varied during biotite crystallization.

Hornblende

Hornblende occurs in Fish Canyon magma as euhedral, generally poikilitic, phenocrysts (0·5–3 mm), without evidence for reaction with the surrounding melt (Fig. 6). An extensive electron microprobe dataset of amphibole compositions (2146 analyses) collected from multiple samples of all units of the Fish Canyon magmatic system defines significant major element variability. The vast majority (>90%) are hornblende *sensu stricto*, but the most alkali-rich and silica-poor analyses reach the edenite field. The overall dispersion is extended toward pargasite by one texturally distinct resorbed core in a large hornblende phenocryst in a Pagosa Peak Dacite sample (PCB1). Excluding this pargasitic core, which we interpret as a relic from an earlier magmatic stage, variations up to 4 wt % absolute for Al_2O_3, and 6 wt % for SiO_2 are observed. When plotted against silica, Al_2O_3, FeO_{tot}, MgO, MnO, TiO_2, Na_2O, and K_2O define linear arrays with negative slopes, except for MgO and MnO, which correlate positively with SiO_2 (Fig. 8). The hornblende grown by Johnson & Rutherford (1989*a*) in an experiment at 2 kbar and 780°C and the composition of their natural hornblende analysis plot near the average of the new dataset.

Fourteen high resolution (5–10 μm point spacing) microprobe traverses across large euhedral hornblende grains record significant internal major element variability. A majority of these traverses (nine) record rimward increases in Al_2O_3, FeO_{tot}, TiO_2, Na_2O, and K_2O, which are compensated by decreases in MgO, MnO, and SiO_2. Typical near-core compositions have Al_2O_3 contents ranging from 5 to 6 wt % absolute, whereas rim compositions reach 7·5–8·5 wt % Al_2O_3 (Fig. 9). Oscillatory zoning ($\sim$10–20 μm wide with amplitude up to $\pm$1 wt % Al_2O_3 in some phenocrysts) is superimposed on the rimward

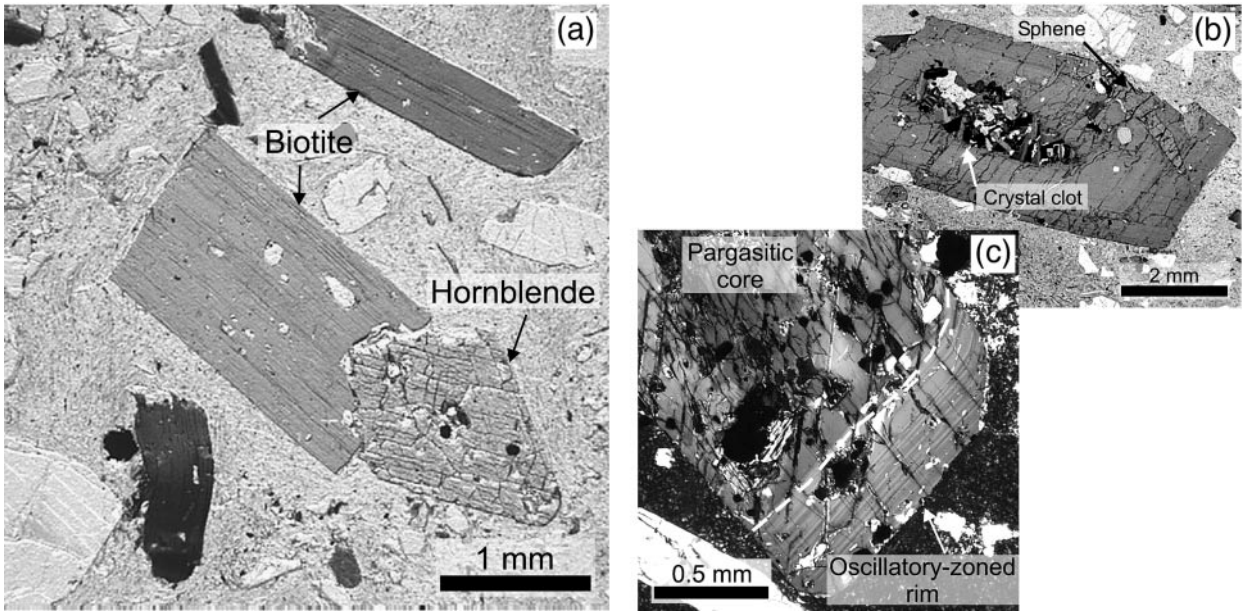

Fig. 6. Hornblende and biotite phenocrysts in Fish Canyon magma. (a) Euhedral to subhedral hornblende and biotite phenocrysts in the Pagosa Peak Dacite (Bfc 171; plane-polarized light). (b) Large hornblende containing a complex core composed of an intergrowth of plagioclase, biotite, and oxides, as well as smaller hornblendes, which are compositionally indistinguishable from the overgrowth. A large euhedral sphene crystal is also included in the hornblende rim (Bfc 68; plane-polarized light). (c) Large hornblende phenocryst showing an oscillatory zoned rim and a pargasitic core (PCB1; partially crossed polars).

zoning. The fine-scale oscillations are characterized by the same strong correlations between all major elements: the zoning profiles of Al_2O_3, FeO_{tot}, TiO_2, Na_2O, and K_2O are nearly parallel, whereas the profiles of MgO, MnO, and SiO_2 are mirror images. This striking interdependence indicates that the same coupled substitutions are responsible for both the oscillations and the core-to-rim trends.

The thermobarometric potential of Al content in hornblendes in near-solidus silicic magmas has been assessed in a number of studies (e.g. Hammarstrom & Zen, 1986; Hollister *et al.*, 1987; Blundy & Holland, 1990; Vyhnal *et al.*, 1991; Schmidt, 1992; Holland & Blundy, 1994; Anderson & Smith, 1995; Anderson, 1996; Ague, 1997), and notably on Fish Canyon material by Johnson & Rutherford (1989*b*) in the first experimental calibration of the Al-in-hornblende barometer. The Al zoning recorded by microprobe traverses across Fish Canyon hornblendes is explored in more detail in a companion paper (Bachmann & Dungan, 2002), but the main characteristics of the profiles are summarized here. The dominant substitution controlling Al variations is the edenite exchange [$Si^T + \square^A \rightleftharpoons Al^T + (Na + K)^A$], but it is coupled with a less important Ti-Tschermak exchange ($Si^T + Mn^{M1–M3} \rightleftharpoons Al^T + Ti^{M1–M3}$); both are inferred to be temperature sensitive (Czamanske & Wones, 1973; Spear, 1981; Blundy & Holland, 1990). In contrast, the pressure sensitivity of the Al-Tschermak substitution ($Si^T + Mg^{M1–M3} \rightleftharpoons Al^T + Al^{M1–M3}$), demonstrated using Fish Canyon material by Johnson & Rutherford (1989*b*), does not play a role in increasing the Al content of natural Fish Canyon amphibole, as $Al^{M1–M3}$ is <0·2 atom p.f.u. and does not correlate significantly with other components. Moreover, if Al_{tot} content in Fish Canyon hornblende were primarily controlled by pressure, an increase toward crystal rims would translate dynamically into a foundering magma chamber. The minimum depth implied by hornblende with ~6 wt % Al_2O_3 would have been shallower than 3–5 km (<1 kbar at 760°C and <1·7 kbar at 700°C), using the recent recalibration of the Al-in-hornblende barometer of Anderson & Smith (1995). In contrast to this geologically unrealistic scenario, temperatures calculated using the geothermometric algorithm of Holland & Blundy (1994; edenite–richterite thermometer) at 2·25 kbar pressure increase from 708 ± 10°C for an Al_2O_3 content of ~6 wt % and An_{28} plagioclase, the typical values of inner parts of hornblende and plagioclase phenocrysts, to 756 ± 15°C for outermost rim compositions (~7·7–8·0 wt % Al_2O_3) with An_{33} plagioclase. These calculated temperatures are realistic, and the temperature obtained from the rim composition is indistinguishable from independent determinations using the Fe–Ti oxide thermometer (760 ± 30°C; Johnson & Rutherford, 1989*a*) or quartz–magnetite oxygen thermometry (762 ± 10°C, I. N. Bindeman, unpublished data, 2001). These zoning profiles are, there-

Table 3: Average biotite compositions from the Fish Canyon magma

	Av. PPD (n = 533)	Av. FCT (O) (n = 271)	Av. FCT (I) (n = 255)	Av. NCD (n = 21)	Av. Gran. xeno. (n = 138)
SiO_2	36·77 ± 0·62	36·86 ± 0·44	36·37 ± 0·58	37·53 ± 0·39	37·67 ± 0·78
TiO_2	4·50 ± 0·10	4·56 ± 0·09	4·57 ± 0·11	4·47 ± 0·09	4·27 ± 0·23
Al_2O_3	13·19 ± 0·24	13·22 ± 0·15	13·30 ± 0·22	13·40 ± 0·29	12·97 ± 0·23
FeO_{tot}	16·31 ± 0·59	16·33 ± 0·60	16·92 ± 0·92	17·37 ± 0·67	15·50 ± 0·71
MnO	0·36 ± 0·04	0·35 ± 0·04	0·37 ± 0·04	0·34 ± 0·05	0·53 ± 0·06
MgO	14·14 ± 0·34	14·01 ± 0·32	13·54 ± 0·64	13·38 ± 0·56	14·70 ± 0·58
BaO	0·07 ± 0·22	0·05 ± 0·14	0·02 ± 0·05	n.a.	0·01 ± 0·02
CaO	0·23 ± 0·13	0·41 ± 0·41	0·28 ± 0·10	0·04 ± 0·05	0·27 ± 0·44
Na_2O	0·40 ± 0·06	0·39 ± 0·06	0·36 ± 0·09	0·46 ± 0·05	0·44 ± 0·07
K_2O	9·35 ± 0·28	9·24 ± 0·27	9·47 ± 0·22	8·98 ± 0·27	9·32 ± 0·16
F	1·08 ± 0·38	1·08 ± 0·44	0·98 ± 0·21	0·77 ± 0·30	1·47 ± 0·34
Cl	0·19 ± 0·02	0·20 ± 0·03	0·20 ± 0·02	0·16 ± 0·02	0·20 ± 0·03
O = F	0·46 ± 0·16	0·46 ± 0·18	0·41 ± 0·10	0·33 ± 0·13	0·62 ± 0·14
O = Cl	0·04 ± 0·01	0·05 ± 0·01	0·05 ± 0·01	0·04 ± 0·00	0·05 ± 0·01
Sum Ox%	96·10 ± 0·67	96·21 ± 0·70	95·90 ± 0·46	96·57 ± 0·63	96·69 ± 0·66
Si	5·05 ± 0·10	5·07 ± 0·08	5·01 ± 0·07	5·18 ± 0·08	5·18 ± 0·12
Ti	0·47 ± 0·01	0·47 ± 0·01	0·47 ± 0·01	0·46 ± 0·01	0·44 ± 0·02
Al	2·14 ± 0·04	2·15 ± 0·04	2·16 ± 0·04	2·18 ± 0·05	2·10 ± 0·05
$Fe^{2+equ.}$	1·87 ± 0·08	1·88 ± 0·08	1·95 ± 0·12	2·01 ± 0·08	1·78 ± 0·09
Mn	0·04 ± 0·00	0·04 ± 0·00	0·04 ± 0·00	0·01 ± 0·01	0·06 ± 0·01
Mg	2·90 ± 0·07	2·88 ± 0·07	2·78 ± 0·12	2·76 ± 0·12	3·01 ± 0·11
Ba	0·01 ± 0·01	0·01 ± 0·02	0·00 ± 0·01	n.a.	0·01 ± 0·01
Ca	0·01 ± 0·03	0·02 ± 0·02	0·02 ± 0·01	0·01 ± 0·00	0·01 ± 0·00
Na	0·11 ± 0·02	0·10 ± 0·02	0·10 ± 0·02	0·12 ± 0·01	0·12 ± 0·02
K	1·64 ± 0·05	1·62 ± 0·05	1·66 ± 0·05	1·58 ± 0·05	1·63 ± 0·03
F	0·47 ± 0·16	0·47 ± 0·19	0·43 ± 0·09	0·34 ± 0·13	0·64 ± 0·15
Cl	0·05 ± 0·01	0·05 ± 0·01	0·05 ± 0·01	0·04 ± 0·00	0·05 ± 0·01

Mineral formulae calculated as 22 equivalent oxygen. H_2O calculated by subtracting the sum from 100. Averages were calculated on the basis of all analyses included in Figs 7 and 21. Electron microprobe analyses performed at the University of Lausanne (O. Bachmann analyst, helped by F. Bussy). Biotite and hornblende: 15 kV, 15 nA, magnification 200 000. Feldspars: 15 kV, 15 nA, magnification 200 000. Glass: 15 kV, 10 nA, magnification 50 000 on raster mode. PPD, Pagosa Peak Dacite; FCT, Fish Canyon Tuff; NCD, Nutras Creek Dacite; I, intracaldera; O, outflow; Gran. xeno., granodioritic xenolith. Standards used were all mineral standards. n.a., not analyzed.

fore, consistent with hornblende crystallization during nearly isobaric reheating. Increasing f_{H_2O} may also have played a role in this rimward increase in Al (Scaillet & Evans, 1999).

Quartz

As noted previously by Lipman *et al.* (1978) and Whitney & Stormer (1985), quartz occurs as large (up to 5–6 mm in diameter) ameboid grains, deeply dissected by melt channels and pools (Fig. 10a). All three Fish Canyon units display these anhedral quartz textures, but they are particularly obvious in the Pagosa Peak Dacite and the Nutras Creek Dacite, wherein crystal shattering was less pervasive.

Plagioclase

Plagioclase displays diverse textures, showing both internal and marginal resorption as well as oscillatory-zoned euhedral overgrowths on volumetrically minor partially resorbed cores (Fig. 10c). Plagioclase phenocrysts have compositions ranging mainly from An_{25} to An_{35}, although a few volumetrically minor more calcic cores have compositions up to An_{75} (Table 4). Despite the fact that high-anorthite cores were not analyzed in the Nutras Creek Dacite,

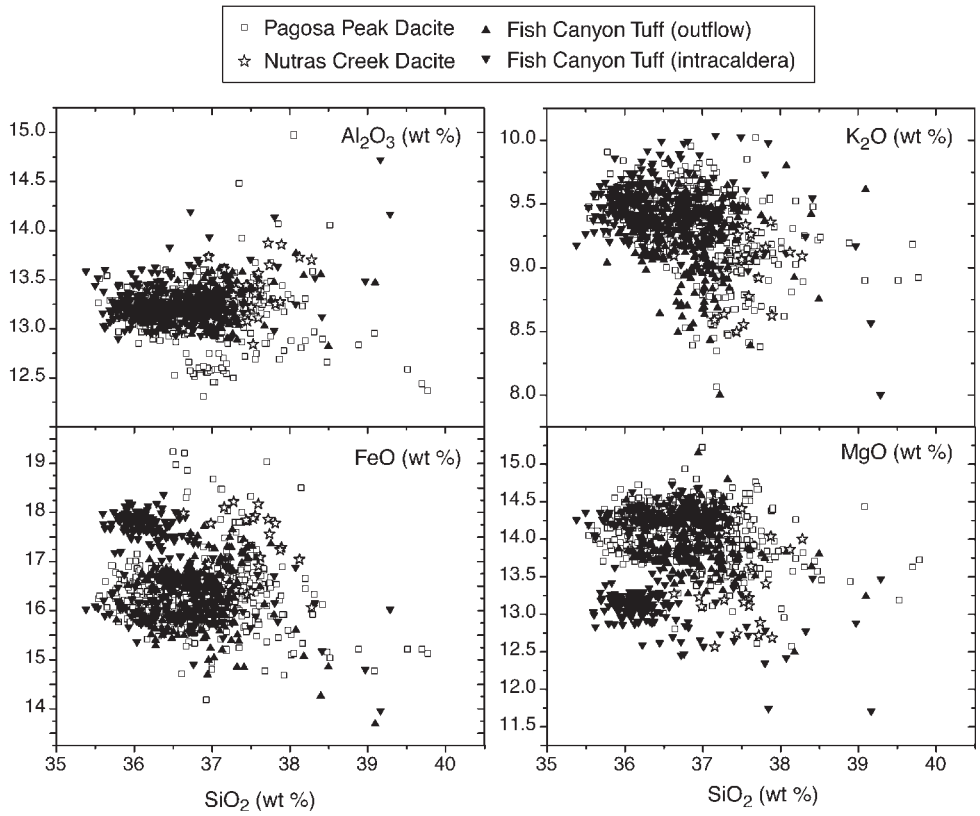

Fig. 7. Major element variation diagrams for biotite (electron microprobe) in each of the stratigraphic units of the Fish Canyon magmatic system. It should be noted that fields overlap extensively for all plotted major elements.

because of the relative paucity of plagioclase analyses in this unit, plagioclase compositions are similar in all three units of the Fish Canyon magmatic system. Oscillatory-zoned rims on plagioclase phenocrysts have two important chemical characteristics that were not noted previously (Fig. 11). First, the background trend progressively rises to more calcic average compositions, from $\sim An_{27-28}$ in grain interiors to $\sim An_{32-33}$ at rims. Second, narrow ($\sim 10\,\mu m$ wide) excursions to more calcic compositions (up to An_{40}) following dissolution surfaces periodically interrupt the typical background trend.

Sanidine

Texturally, sanidine in the Fish Canyon magma is very similar to quartz (Fig. 10b). It also occurs dominantly as large (2–5 mm) ameboid grains in all three units of the Fish Canyon magmatic system, although efficient crystal shattering and dispersal related to magma fragmentation and emplacement has rendered primary grain morphologies obscure in the Fish Canyon Tuff. In contrast to quartz, many of the extensively resorbed sanidine grains contain inclusions of other mineral phases. Plagioclase is by far the most abundant, but hornblende, biotite, Fe–Ti oxides, apatite, and sphene are also present in minor quantities. Plagioclase inclusions in these poikilitic sanidines are of two types (Fig. 12), both having the same compositions as the euhedral overgrowths on plagioclase phenocrysts ($An_{30\pm3}$). The first consists of irregularly shaped grains, which are in optical continuity despite being physically isolated (Fig. 12a–c). These inclusions range in size from a few microns to ~ 1 mm, they are generally subequant with irregular outlines (Fig. 12a–c), and they are preferentially concentrated near the rims of large sanidine crystals (Fig. 12b). Inclusions of the second type are subhedral–euhedral laths up to 1 mm long, characterized by thin melt zones along contacts with sanidine (Fig. 12c and d).

In addition to the marginal and internal resorption textures and multiple types of mineral and glass inclusions, many Fish Canyon alkali feldspars are conspicuously zoned, mainly in the outer parts of crystals (Fig. 13). Optical zoning is manifested as bands of 0·1–1 mm width with internally variable and slightly different extinction angles from the unzoned cores of the crystals. Whereas these bands are generally subparallel to anhedral grain boundaries, their morphology is more irregular than euhedral growth zoning (i.e. planar crystal faces). Where multiple bands are present,

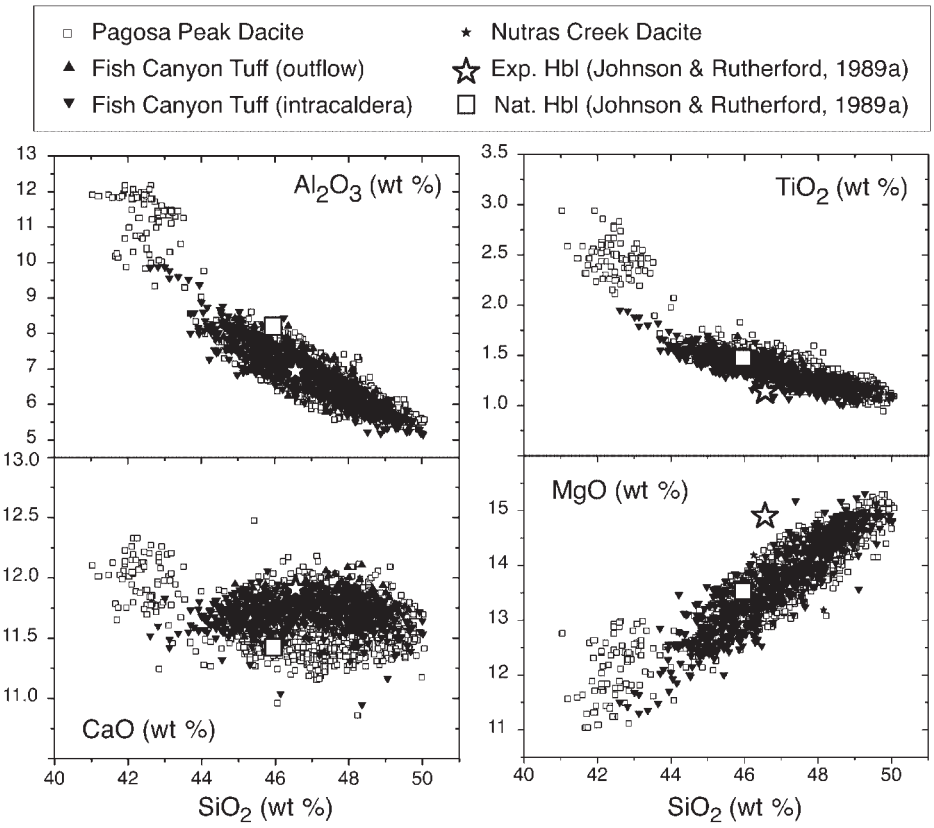

Fig. 8. Major element variation diagrams for hornblendes from each stratigraphic unit of the Fish Canyon magmatic system. Data from the granodioritic xenolith are not shown. The natural and experimental hornblende compositions reported by Johnson & Rutherford (1989*a*) are plotted for comparison. The experimental product plots close to the average Fish Canyon hornblende composition for most elements. (Note the overlap between amphibole compositions from the various Fish Canyon stratigraphic units, except for the distinctive pargasitic core, which we interpret as a relic inherited from an earlier event.)

an undulatory surface commonly truncates earlier bands, suggesting dissolution (Fig. 13b and d). Celsian (Cn) increases by a factor of 2 mol % absolute, immediately outside the zoning boundaries, balanced mainly by decreases in Or and increases in Ab (Fig. 14). Within each zone, Cn then decreases progressively to its background value (~2 mol %), accompanied by a decrease in Or and an increase in Ab (Fig. 14a, Table 5). In phenocrysts containing multiple juxtaposed zones, Cn variations define sawtooth profiles, with abrupt re-establishments of high Cn content across zoning boundaries, followed by linear decreases (Fig. 14b; fig. 5 of Lipman *et al.*, 1997). Sanidines characterized by variable Cn content are invariably poikilitic, containing swarms of isolated plagioclase inclusions in optical continuity [Figs 12b and c, 13, 14a, and 20b (below)], but such inclusions are absent from adjacent unzoned cores.

Fine-scale granophyric intergrowths of quartz and K-feldspar with planar terminations against adjacent melt occur as overgrowths around pre-existing feldspar crystals in late-erupted northern and central intracaldera Fish Canyon Tuff, and in the Nutras Creek Dacite (Lipman *et al.*, 1997). Granophyre is a late magmatic feature, as it has faceted crystal faces and it fills open fractures in broken host crystals, thought to have been partly disrupted by expansion of melt inclusions during rapid decompression related to the early Fish Canyon eruptions (Fig. 15; Best & Christiansen, 1997; Lipman *et al.*, 1997). An important feature, not mentioned by Lipman *et al.* (1997), is that granophyric overgrowths appear to have preferentially nucleated on sanidines displaying bands of variable Cn content riddled with plagioclase inclusions in optical continuity.

Accessory phases

Accessory phases in the Fish Canyon magma (sphene, Fe–Ti oxides, apatite, zircon, pyrrhotite) are generally euhedral. Sphene, Fe–Ti oxides, apatite, and zircons are all found as inclusions in the major phases and in the interstitial glass. Pyrrhotite is rare and uniquely present as inclusions, mainly in magnetite (Whitney & Stormer, 1985). The largest sphene and Fe–Ti oxide grains can reach

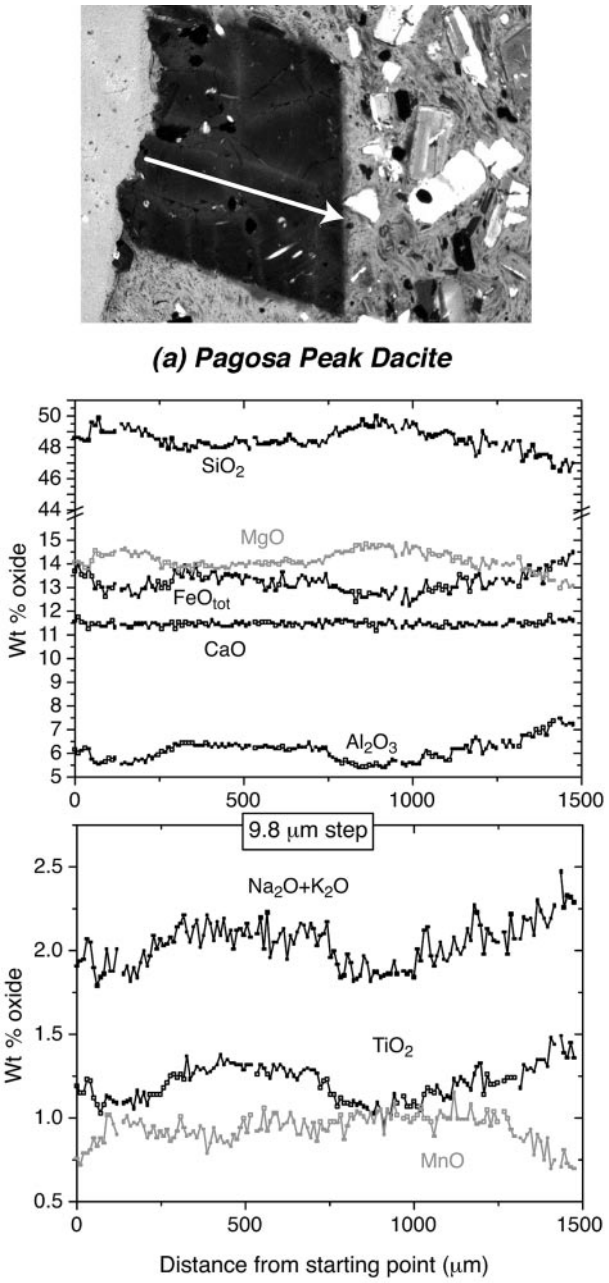

Fig. 9. Electron microprobe traverse (core to rim) across one large hornblende phenocryst in the Pagosa Peak Dacite (Bfc 196a; partially crossed polars). The crystal has been truncated at the edge of the thin section. The area between 200 and 600 μm probably represents the core composition of this crystal. The profiles of the oxides shown here are either sub-parallel (Al_2O_3–FeO_{tot} and MgO–SiO_2) or are equally good mirror images (e.g. Al_2O_3–SiO_2 and Fe_2O_3–SiO_2). The Na_2O + K_2O, and TiO_2 profiles are sub-parallel to the Al_2O_3 profile, whereas MnO is its mirror image. Thus, it would appear that the same coupled substitutions dominate throughout the profiles and that both the long-wavelength trends and fine-scale oscillations were caused by the same factors.

0·5 mm in size, whereas the other phases are generally smaller than 50 μm. We have not undertaken mineral chemistry analyses of these phases.

PETROLOGICAL IMPLICATIONS

Reverse zoning in plagioclase overgrowths

The major element composition of plagioclase is controlled by pressure, temperature, and melt composition, including a major dependence on H_2O content (Rutherford & Devine, 1988; Housh & Luhr, 1991). The reverse compositional zoning trend over hundreds of microns in the plagioclase rims requires a progressive change in one or more of these parameters. As for rimward increases of Al in hornblende, heating could have conceivably played a role in the development of these zoning profiles, but changes in melt chemistry (increased Ca and/or H_2O as a result of interactions with less evolved melt) may have also contributed to the overall reverse trend and calcic spikes. Calcic cores in plagioclase probably represent relics from an earlier magmatic stage.

Plagioclase inclusions in optical continuity associated with Ba zoning in sanidine: Rapakivi textures

One process potentially capable of generating oriented plagioclase inclusions in K-feldspar is phase unmixing at the solvus (exsolution). However, the diversity of sizes and the irregular subequant shapes of the inclusions set them apart from any exsolution textures described in the literature (e.g. Smith, 1974). An alternative hypothesis, proposed by Stimac & Wark (1992) to explain similar textures in silicic lavas of Clear Lake, California, is epitaxial nucleation and growth of plagioclase at many points on the periphery of sanidine, followed by regrowth of sanidine in the interstices between plagioclase grains. The Clear Lake silicic lavas show multiple examples of well-developed plagioclase mantles on sanidine (i.e. Rapakivi textures; Sederholm, 1891), into which these poikilitic zones grade, and the inference that these inclusions are related to plagioclase mantling is straightforward. Although complete plagioclase mantles are rare in Fish Canyon magma, multiple grains of plagioclase with a common optical orientation attached to the rims of large sanidine crystals are preserved in a few samples (Fig. 16), hinting at remnants, and/or incipient formation, of discontinuous plagioclase mantles.

The spatial association of plagioclase inclusions in optical continuity with large variations in Ba/K in the host sanidine was also noted by Stimac & Wark (1992) in the mixed Clear Lake lavas, and these manifestations in the Fish Canyon magma strongly support the interpretation that the discontinuous plagioclase mantles were engulfed during renewed growth of K-feldspar, as demonstrated experimentally by Wark & Stimac (1992). In this context, the oscillatory Ba zoning associated with dissolution surfaces in sanidines are more readily explained by multiple episodes of K-feldspar growth rather than the development

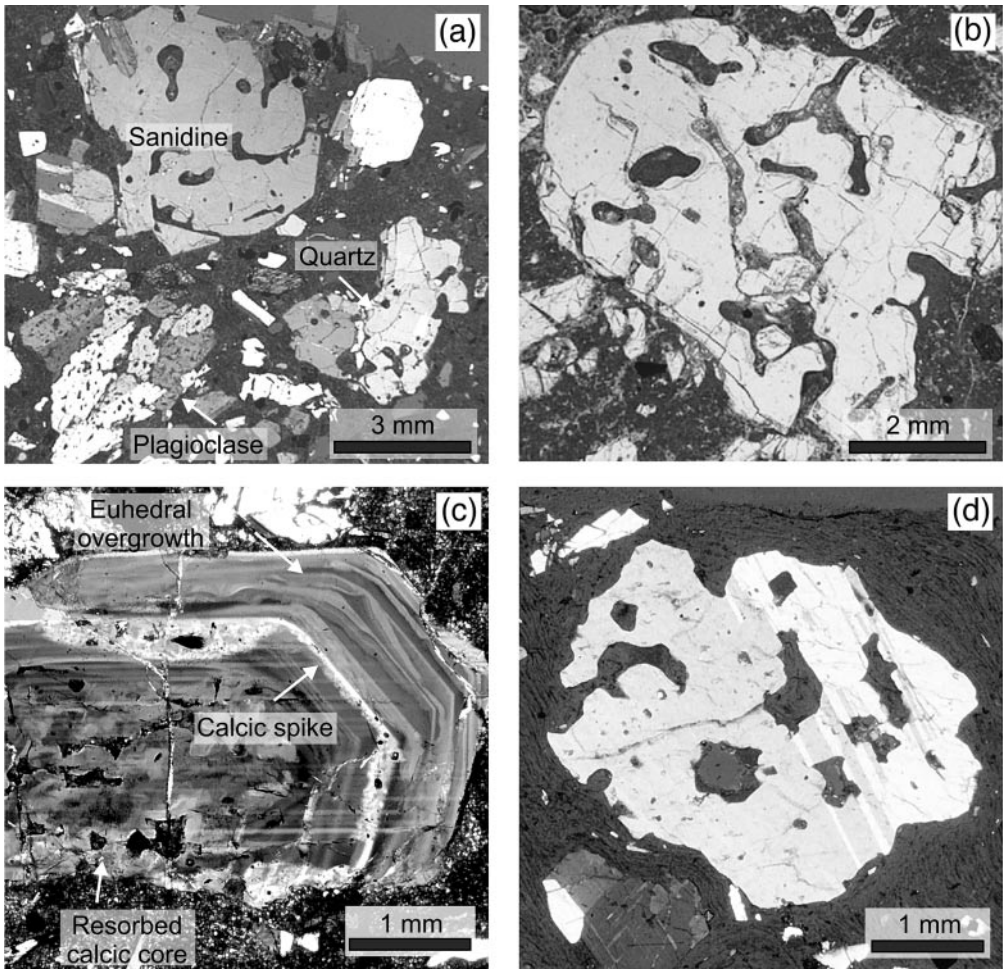

Fig. 10. Textures in feldspars and quartz in non-fragmented Fish Canyon magma. (a) Sanidine, plagioclase and quartz phenocrysts in the Nutras Creek Dacite, all showing anhedral outlines and internal melt channels connected to the matrix (Bfc 115c; crossed polars). (Note also plagioclase phenocrysts, to the left and to the right of the large sanidine, which are euhedral and lack resorption textures.) (b) Large, anhedral sanidine in the Pagosa Peak Dacite (PCB1; partially crossed polars). (c) Complexly zoned plagioclase in the Pagosa Peak Dacite, wherein a euhedral mantle displaying oscillatory growth zoning has overgrown a partly resorbed core (Bfc 12; crossed polars). (Note the prominent 'calcic spike' immediately outboard of the resorption surface that marks the boundary between the core and the overgrowth.) (d) Corroded plagioclase grain in the Pagosa Peak Dacite (Bfc 171; partially crossed polars). Euhedral terminations are never observed on sanidine and quartz, but are the rule rather than the exception on plagioclase.

of oscillatory zoning following repeated mixing with a more Ba-rich andesitic magma, as proposed by Lipman *et al.* (1997). Evidence of physical mixing between silicic and mafic magmas is scarce in the Fish Canyon magmatic system, and the spatial association of cyclic zoning in sanidine with the oriented plagioclase inclusions is more readily explained by repeated episodes of plagioclase mantling followed by sanidine reprecipitation. However, the possibility of some addition of Ba from a less evolved melt cannot be ruled out. Mass-balance considerations, based on the volume ratio of zoned sanidine to plagioclase inclusions (>5:1), tend to suggest that some Ba was contributed from an external source, in accord with the presence of calcic spikes in the euhedral plagioclase overgrowths. An alternative explanation for the large volume ratio of zoned sanidine vs plagioclase inclusions in the Fish Canyon magma is partial dissolution of the plagioclase mantles before sanidine regrowth. This mechanism could also explain the highly irregular contours of the plagioclase inclusions, and would be consistent with the partly corroded and discontinuous plagioclase mantles shown in Fig. 16.

Inclusions of plagioclase laths and grain-boundary melting

The textural relations of the subhedral–euhedral plagioclase laths with their host sanidine phenocrysts are in sharp contrast to the oriented plagioclase inclusions, implying a different origin. These inclusions were probably free

Table 4: Representative plagioclase analyses from the various units of the Fish Canyon magmatic system

	Core PPD	Core FCT	Rim PPD	Rim FCT	Rim NCD	Rim FC xeno.	Outermost rim FC xeno.
SiO_2	48·23	49·00	59·98	61·35	60·09	59·64	63·12
Al_2O_3	32·11	32·41	24·74	23·36	25·31	25·24	22·46
FeO_{tot}	0·27	0·37	0·20	0·24	0·06	0·08	0·05
CaO	15·63	15·70	6·69	5·68	6·72	6·64	3·87
BaO	0·01	0·00	0·05	0·00	0·02	0·07	0·00
Na_2O	2·71	2·65	7·51	7·60	7·52	7·52	8·62
K_2O	0·14	0·10	0·74	1·10	0·44	0·54	0·95
Sum Ox%	99·10	100·23	99·90	99·33	100·36	99·89	99·20
Ab	23·65	23·29	64·19	66·29	65·24	65·04	75·72
An	75·53	76·16	31·60	27·39	32·21	31·75	18·76
Or	0·80	0·55	4·13	6·31	2·52	3·08	5·51
Cn	0·02	0·00	0·08	0·00	0·03	0·13	0·00

phenocrysts that were engulfed by sanidine. The occurrence of thin melt zones at the contacts between the two phases and the absence of Ba zoning associated with these inclusions suggest that grain boundary melting occurred after the establishment of solid–solid contacts following engulfment and that sanidine did not regrow subsequently.

Quartz inclusions in feldspars

In spite of the fact that we do not observe quartz inclusions in feldspars, we infer that included quartz was present at some stage in the evolution of the Fish Canyon magma, but that it subsequently melted. Secondary SiO_2 reprecipitation in internal melt channels within sanidine is ubiquitous, and we have documented an inclusion of 95–96 wt % SiO_2 glass (+ ~2 wt % Al_2O_3 and <1 wt % CaO, Na_2O, and K_2O) in a plagioclase phenocryst (Fig. 17). Silica reprecipitation in Fish Canyon magma is not hydrothermal, as it occurs in vitrophyric samples and it is restricted to melt channels in feldspars. Thus, both of these manifestations reflect the formation of SiO_2-rich melts within host feldspars.

Disequilibrium affecting quartz and both feldspars supports the inference of a pre-eruptive temperature and/or H_2O increase. Dissolution of quartz alone can result

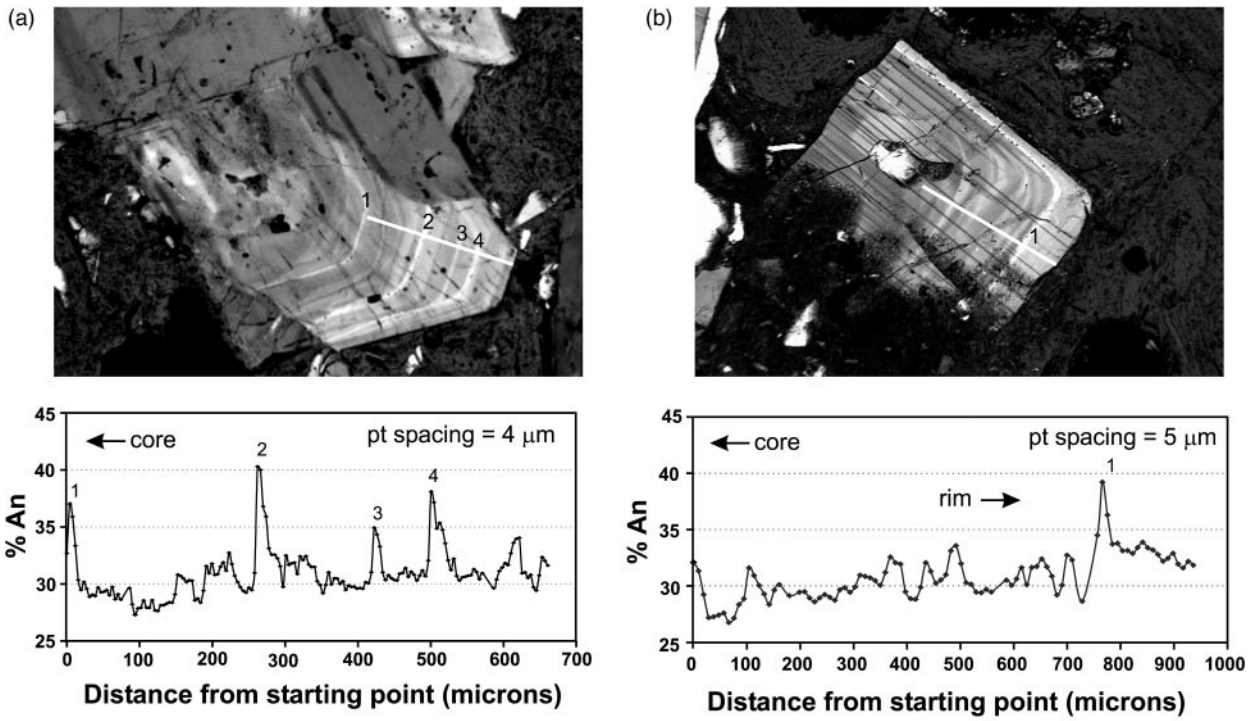

Fig. 11. High-resolution electron microprobe traverses across two plagioclase phenocrysts with euhedral, oscillatory zoned mantles. (a) Pagosa Peak Dacite, Bfc 59; (b) Fish Canyon Tuff, Bfc Fv (both with crossed polars). Both compositional profiles shown here are typical of euhedral plagioclase in Fish Canyon magma. In both cases, the main features are oscillatory zoning marked by abrupt 'calcic spikes' up to An_{40}, which are superimposed on an increase in the baseline level from ~$An_{27–28}$ to ~$An_{32–33}$.

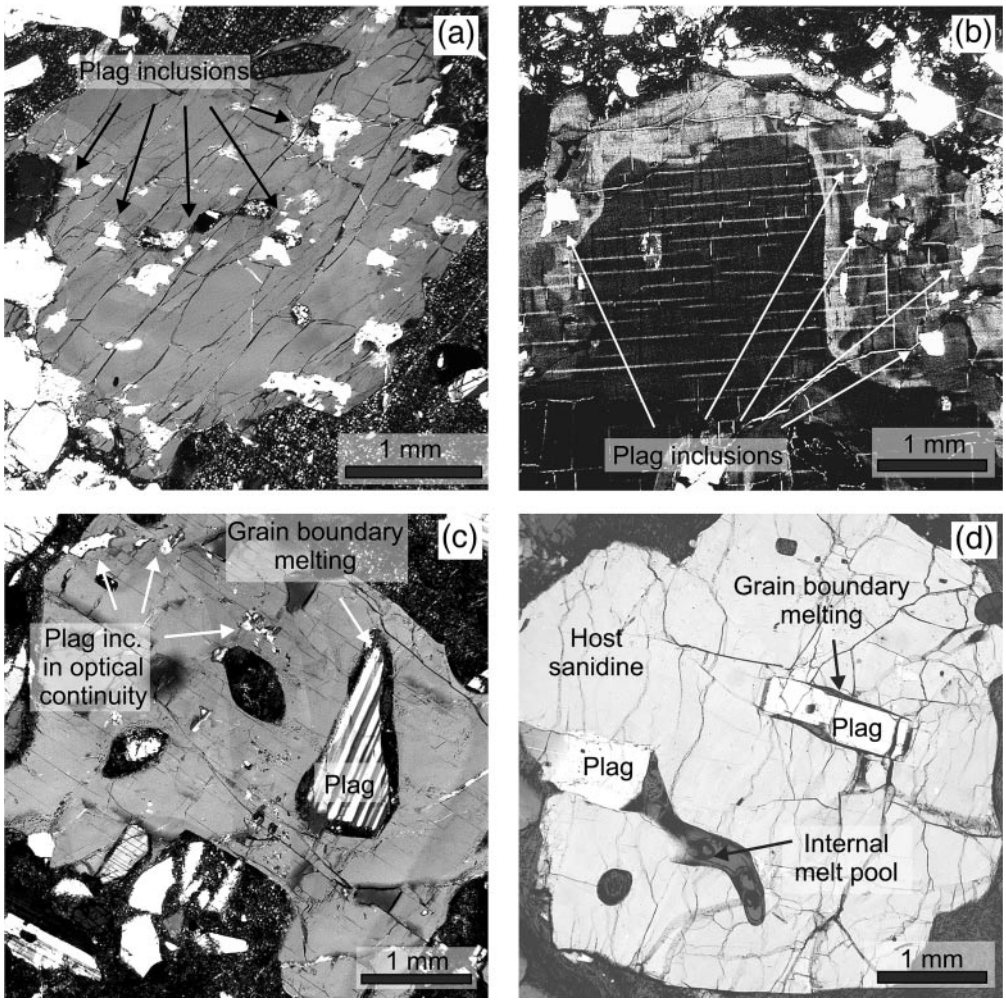

Fig. 12. Two types of plagioclase inclusions in Fish Canyon sanidines. (a, b) Multiple isolated, anhedral inclusions in optical continuity, showing a range of sizes from a few microns to 0·5 mm (PCB1 and Bfc 171; crossed polars). In (b), inclusions are concentrated at the rim of the sanidine and they are spatially associated with large oscillatory variations in Cn content (Ba) of the host sanidine. In contrast, the core (delimited by an undulatory resorption surface) is both unzoned and free of inclusions. (c) and (d), examples of sanidine containing larger subhedral–euhedral plagioclase laths. These are typical of the second type of inclusions. This second population is commonly associated with incipient dissolution of both phases (i.e. grain boundary melting) along the contact with the host sanidine (Bfc 12 and Bfc 91; crossed polars). The sanidine in (c) contains both populations.

from magma depressurization as the quartz stability field contracts relative to feldspars in the Qz–Ab–Or ternary phase diagram with decreasing pressure (e.g. Tuttle & Bowen, 1958), but volumetrically important dissolution affecting all three phases is incompatible with adiabatic ascent of water-rich magmas.

Granophyre overgrowths

To explain occurrences of granophyre uniquely in the late-erupted units of the Fish Canyon magmatic system, Lipman *et al.* (1997) proposed that granophyre crystallization was induced by the early eruptions from the Fish Canyon magmatic system (both Pagosa Peak Dacite and early Fish Canyon Tuff). Rapid decompression and devolatilization of the remaining magma upon eruption of the upper part of the chamber produced near-instantaneous, isothermal undercooling that triggered this distinctive type of crystallization. The same mechanism has also been proposed for the formation of granophyre-bearing xenoliths in the Alid volcanic field (Lowenstern *et al.*, 1997).

The association of granophyre with Rapakivi textures has been documented elsewhere (Wahl, 1925; Backlund, 1938; Vorma, 1971), in particular in granites of the Wiborg Massif, Finland, the type locality of Rapakivi granite. The textures in these plutonic examples are similar to those in the Fish Canyon magmatic system, consistent with a genetic relationship between Rapakivi and granophyre formation. In the Fish Canyon magmatic

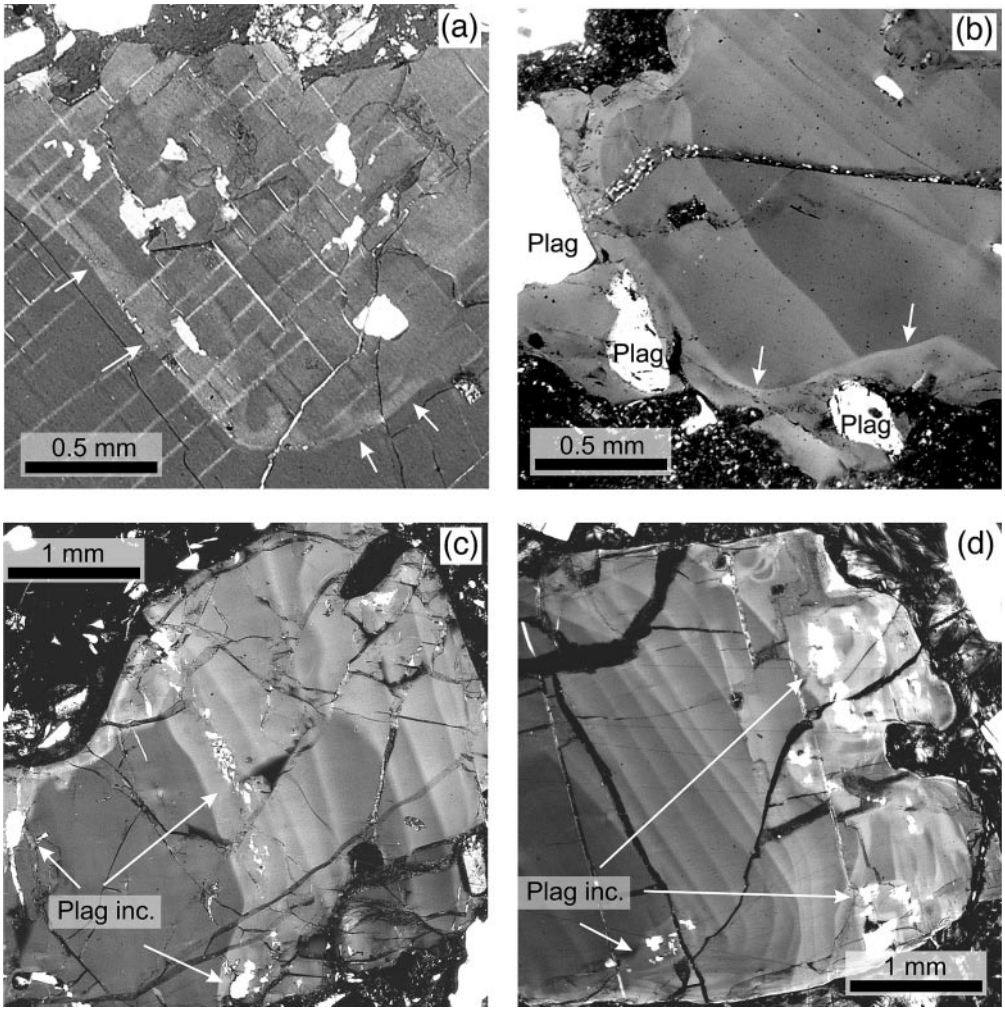

Fig. 13. Fish Canyon sanidines showing compositional zoning associated with plagioclase inclusions in optical continuity (all images with crossed polars). Each band has an innermost Ba-rich zone (light grey), which gives way outward to dark grey sanidine with lower Ba concentrations. (a) Plagioclase inclusions in optical continuity enclosed in the zoned outer part of a large sanidine (inclusions are absent in the homogeneous core—boundary marked by arrows). (b) Truncation of earlier growth bands by an undulatory surface (arrows) suggesting dissolution (Bfc 41). Three optically continuous plagioclase inclusions are preserved in the outermost rim. (c) and (d), two sanidines showing numerous bands in association with plagioclase inclusions in optical continuity (Bfc 31 and 100a). Minerals were partly fractured during polishing.

system, a related crystallization history for both phases of alkali feldspar growth is strengthened by the optical continuity and compositional similarity ($\sim Or_{70–75}$) of granophyric overgrowths and host crystals (Lipman *et al.*, 1997). This association may be a consequence of preferential crystallization of granophyre in the vicinity of Rapakivi crystals, as a result of local enrichment of silica and K-feldspar component in the melt as K-feldspar dissolves and plagioclase crystallizes from this feldspathic melt (Watson, 1982; Wark & Stimac, 1992).

Multiphase glomerocrysts and diffusive re-equilibration

Multiphase glomerocrysts, comprising variable amounts of intergrown feldspars, hornblende, biotite, and oxides, are found in the Fish Canyon magma. These clots are inferred to represent fragments of plutonic material, as they commonly retain solid–solid grain contacts. However, whenever two feldspar phases are in contact, thin melt zones are common along grain boundaries (Figs 12c and d, and 18). These textures resemble those in partially melted granitoid xenoliths entrained in mafic to intermediate lavas (e.g. Grove *et al.*, 1988; Kaczor *et al.*, 1988; Gardner & McPhie, 1999).

The preservation of solid–solid contacts between sanidine and plagioclase in several multiphase aggregates has led us to test whether the complex thermal history that we have inferred is recorded in diffusion-controlled compositional profiles near these grain boundaries. In most grain boundaries that are oriented sub-vertically,

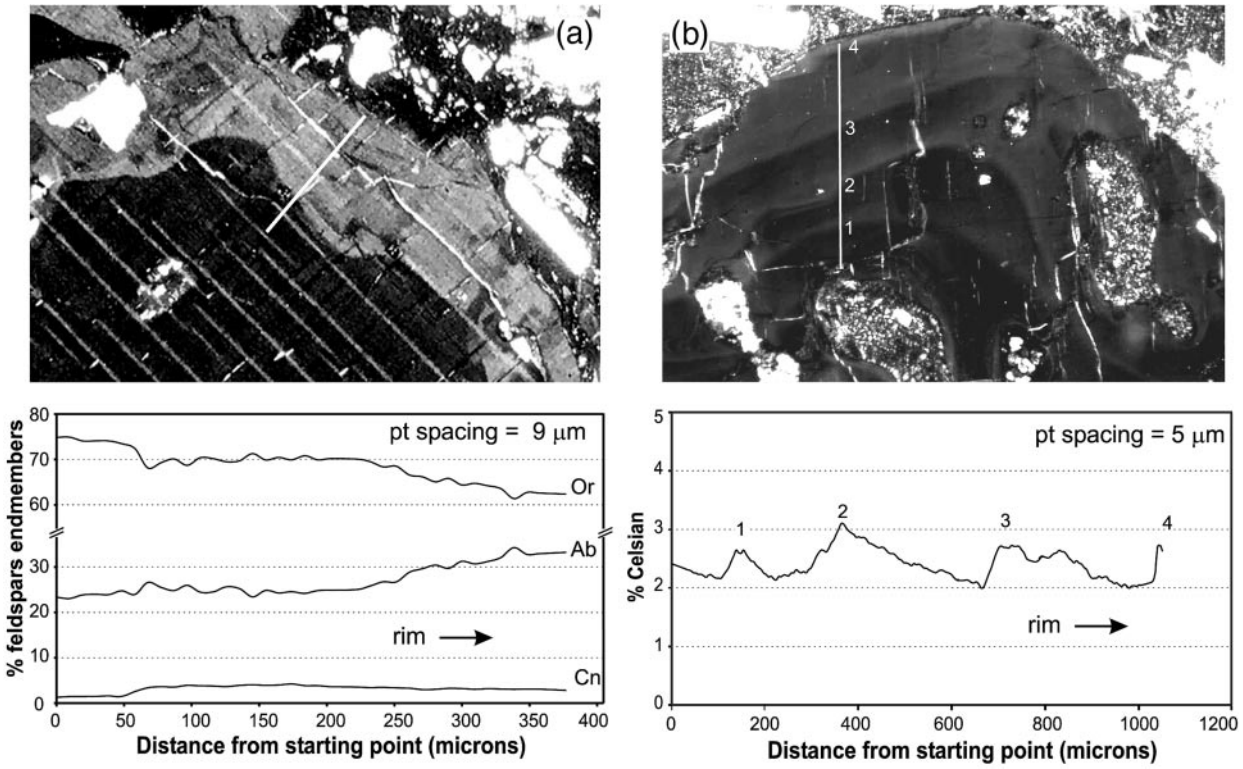

Fig. 14. (a) Electron microprobe traverse across a zoning boundary in a large Pagosa Peak Dacite sanidine (Bfc 171, same as in Fig. 12b), showing a sharp increase in celsian (Cn) (Ba) just outboard the undulating resorption surface, correlated with a decrease in Or and increase in Ab. The trends then define a progressive increase in Ab, correlated with a decrease in Cn and Or away from this surface. This Ba-rich outer zone is thought to represent a second generation of sanidine, which grew from a melt enriched in Ba. The origin of this Ba enrichment in the melt is thought to result directly from the development of Rapakivi textures [see Wark & Stimac (1992) and text for details], as Ba released during sanidine dissolution is not incorporated in the plagioclase structure. Limited addition of Ba from a more mafic magma may also have played a role in the development of this zoning. (b) Electron microprobe traverse across a large sanidine (PCB1; crossed polars) showing abrupt increases in Cn, by up to 1 mol %, across optical zoning boundaries (numbered 1–4). The profile displayed here was slightly smoothed using a running average.

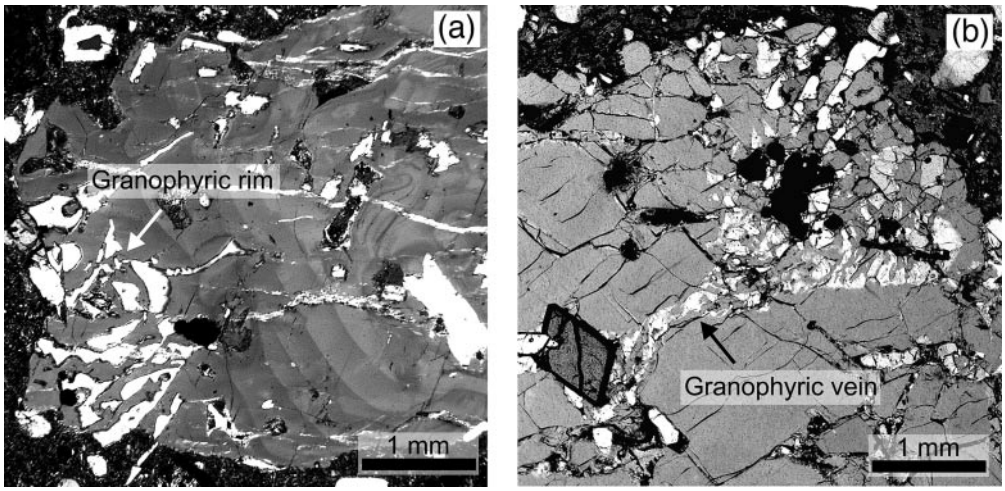

Fig. 15. Granophyric overgrowths on Fish Canyon feldspars (both images with crossed polars). (a) Granophyric rim on a large crystal in the Nutras Creek Dacite associated with multiple broad oscillatory zones, which are spatially associated with plagioclase inclusions in optical continuity and numerous melt pockets (Bfc 115). (b) Granophyre filling a fracture in a sanidine from the late-erupted intracaldera Fish Canyon Tuff. These fractures are thought to result from crystal shattering during decompression of the magma chamber as a result of early eruptions of the Fish Canyon magmatic system (see main text; Bfc 191).

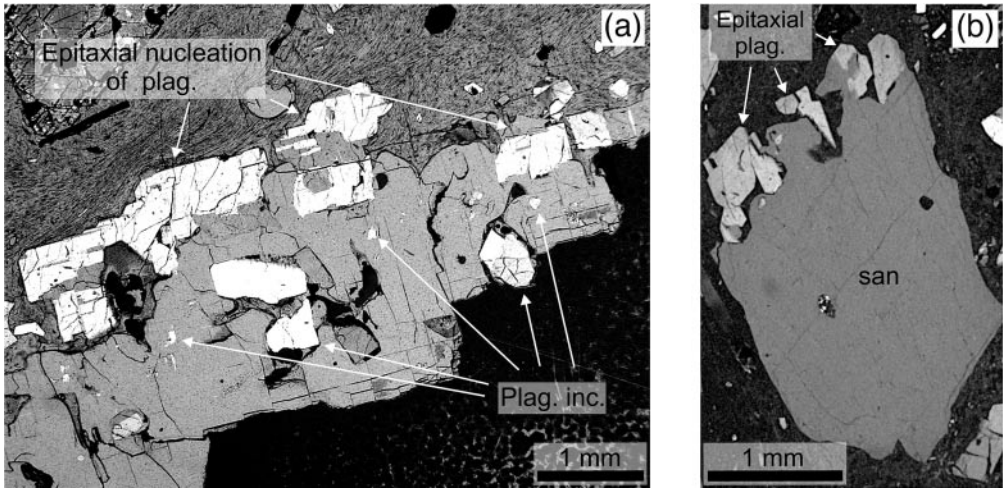

Fig. 16. Discontinuous plagioclase mantles on sanidines in the Pagosa Peak Dacite. (a) The multiple grains of plagioclase intergrown with the outer margin of the associated sanidine are all in optical continuity with each other and with the plagioclase crystals located within this sanidine (Bfc 171; plane-polarized light; lower right margin of the sanidine crystal is truncated at the edge of the thin section). (b) Large grain of resorbed sanidine rimmed on one end by multiple grains of plagioclase, all in optical continuity. We interpret the attachment sites of these grains on sanidine as epitaxial nucleation sites. Plagioclase grains, which are not in contact with sanidine in the plane of this thin section, are still likely to have attained their orientation by epitaxial nucleation. We interpret this grain as an example of the initial stages of formation of Rapakivi-like texture wherein plagioclase mantles form during sanidine dissolution.

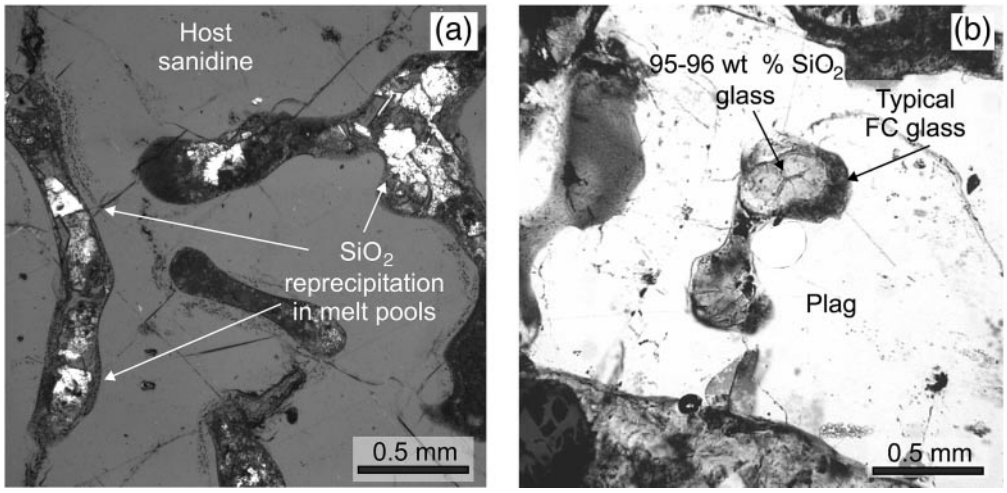

Fig. 17. Evidence for melting of quartz inclusions in feldspar hosts. (a) High-magnification view of the melt channels of the large Pagosa Peak Dacite sanidine shown in Fig. 10b (PCB1). Birefringent multigrain aggregates within melt channels are SiO_2, which we interpret as the product of late reprecipitation from extremely SiO_2-rich melt after melting of quartz inclusions. (b) Complex melt inclusion in a Pagosa Peak Dacite plagioclase. The inner glassy zone marked by the arrow has the composition of 95–96 wt % SiO_2 (+ 1·8–2 wt % Al_2O_3 and <1 wt % CaO, Na_2O and K_2O) whereas the surrounding darker glass has the same composition as typical matrix (Bfc 59; plane-polarized light). We interpret this occurrence as melting of a quartz inclusion and host plagioclase within a melt channel that was connected in three dimensions to the surrounding melt. It should be noted that the volume of melted quartz is approximately equal to the volume of melted plagioclase within this melt pool.

the width of the affected zone is so narrow (<10 μm) that useful information cannot be obtained. Consequently, we have profiled an intact plagioclase–sanidine contact with a subhorizontal orientation (5–10°) relative to the plane of the thin section. This geometry leads to a lateral expansion of compositional gradients so that they can be resolved analytically but it also limits quantitative treatment. This profile traverses the outer margin of a plagioclase grain, beginning in a region with oscillatory magmatic zoning, and then crosses into the grain boundary region where optical zoning is less evident.

The primary magmatic and diffusion-controlled zoning profiles are distinguished by different co-variations in Ab–An–Or (Fig. 18, Table 6). A prominent 'magmatic

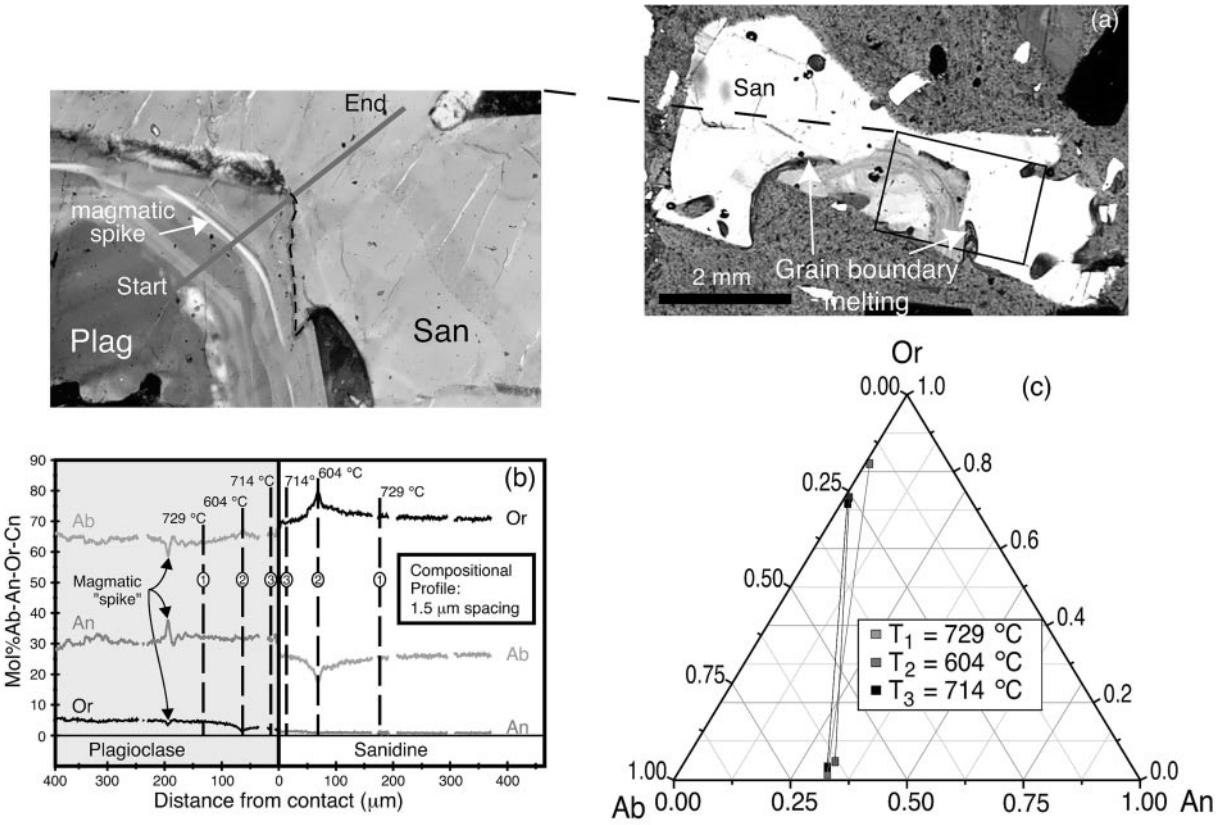

Fig. 18. (a, b) Electron microprobe traverse across a plagioclase–sanidine grain boundary preserved in a microplutonic fragment, designated by the line on the photomicrograph at the top left. This profile shows wave-like compositional zoning on both sides of the contact, interpreted as diffusive Na–K exchange across the grain boundary induced by a thermal fluctuation. (Note the irregular contact, highlighted by the dashed line, suggesting a nearly horizontal interface between the two phases.) (c) Ternary diagram showing the three feldspar pairs chosen on the microprobe profile for the thermometry exercise. T_1 and T_3 have essentially the same compositions and overlap in this diagram. T_2 is shifted toward higher Or in sanidine and lower An in plagioclase, inducing a clockwise rotation of the tie-line, which crosses the other two. Temperatures are calculated using the Solvcalc program of Wen & Nekvasil (1994) and the calibration of Elkins & Grove (1990). (Note grain boundary melting at the contact between the two phases.)

spike' in the plagioclase profile at ~200 μm from the grain boundary shows the expected troughs in Ab and Or associated with a peak in An component. In contrast, the Ab peak located ~70 μm from the grain boundary is not associated with a corresponding decrease in An and it is mirrored by a trough in Or. Significantly, corresponding peaks in Or and Ab have opposite polarities in the adjacent sanidine (i.e. high Or in sanidine mirrors low Or in plagioclase, as well as high Ab in sanidine), again at ~70 μm from the grain boundary and without a complementary change in An. These complex profiles are not readily explained as the products of magmatic crystallization, but a two-stage diffusive exchange history first in response to subsolidus cooling and then in response to reheating is plausible. During cooling, the plagioclase and sanidine exchanged Na and K, whereas divalent Ca remained nearly unchanged, such that the sanidine became more potassic and less sodic (and vice versa for plagioclase). This trend was reversed during a short heating event, and the cooling profiles within ~70 μm of the grain boundary were overprinted by diffusive exchange in the opposite sense, leading to mineral compositions at the contact that are not too different from those in the interiors of the grains.

To provide a qualitative thermal framework for this discussion, we calculated nominal temperatures of coexisting plagioclase–sanidine pairs along this profile. The first pair (1: 729°C) is at the inferred limit of diffusive exchange, and therefore approximates late-stage magmatic crystallization; the second pair (2: 604°C) is situated at the complementary Or–Ab peaks ~70 μm from the grain boundary, and therefore records the impact of cooling; the third pair (3: 714°C) records reheating near the grain boundary. The rotation of the low-temperature tie-lines in the feldspar ternary (Fig. 18c, Table 6) shows the proportionally larger impact of temperature on alkali feldspar relative to plagioclase. Although these temperatures are only a qualitative record of thermal changes

Table 5: Sanidine analyses from microprobe traverse illustrated in Fig. 14b

	~100 mm*	~120 mm (point 1)	~370 mm (point 2)	~500 mm	~670 mm	~690 mm (point 3)
SiO_2	64·02	63·66	63·41	64·60	65·35	64·84
Al_2O_3	18·72	18·79	18·92	18·97	18·75	18·9
FeO_{tot}	0·03	0·06	0·09	0·05	0·07	0·18
CaO	0·17	0·22	0·25	0·16	0·12	0·18
BaO	1·14	1·47	1·76	1·33	1·05	1·56
Na_2O	2·77	2·74	2·81	2·81	2·90	2·89
K_2O	12·46	11·98	12·05	12·25	12·44	12·04
Sum Ox%	99·28	98·92	99·28	100·18	100·69	100·59
Ab	24·50	24·81	24·99	25·01	25·52	25·73
An	0·82	1·08	1·24	0·77	0·59	0·87
Or	72·64	71·42	70·61	71·82	72·02	70·59
Cn	2·05	2·68	3·17	2·40	1·87	2·81

*Approximate distance from starting point on traverse shown in Fig. 14b.

Table 6: Feldspar analyses used to calculate temperatures in Fig. 18

	T1 plag	T1 san	T2 plag	T2 san	T3 plag	T3 san
SiO_2	60·21	64·27	60·31	63·64	59·31	64·35
Al_2O_3	24·13	18·71	24·41	18·31	24·30	18·76
FeO_{tot}	0·23	0·12	0·28	0·18	0·24	0·22
CaO	6·79	0·29	6·56	0·15	6·86	0·20
BaO	0·06	1·61	0·03	1·13	0·05	1·08
Na_2O	7·33	2·88	7·46	1·81	7·89	2·72
K_2O	0·84	11·71	0·22	13·42	0·42	12·08
Sum Ox%	99·59	99·59	99·25	98·66	99·09	99·39
Ab	62·96	25·98	66·42	16·56	65·93	24·76
An	32·21	1·45	32·30	0·78	31·67	0·99
Or	4·73	69·64	1·29	80·58	2·33	72·27
Cn	0·10	2·93	0·04	2·09	0·08	1·98

Temperatures calculated with the feldspar thermometer program Solvcalc (Wen & Nekvasil, 1994), using the Elkins & Grove (1990) calibration. Input parameters: 2 kbar and precision of 0·02 on mole fraction.

in the Fish Canyon magma chamber, the apparently diffusion-related profiles signal the difficulty of documenting coexisting equilibrium feldspars in a magma that shows extensive feldspar resorption textures, and illustrate the problem of uncritical applications of feldspar compositions from such grain boundaries.

GLASS PETROGENESIS

Interstitial glass is devitrified in most cases, but it is preserved in vitrophyres of the Pagosa Peak Dacite and Fish Canyon Tuff. Vitrophyric material is particularly abundant in the Pagosa Peak Dacite, where interstitial melt is typically preserved in large magmatic blobs mainly as Fe-depleted colorless glass containing minute filamental oxide grains (1–2 μm diameter). However, isolated pools (200–500 μm) of brownish glass lacking any crystallization or devitrification products were also found (Fig. 19a and b). Rare pools of similarly homogeneous brown glass are present in a few vitrophyre samples from the outflow and intracaldera facies of the Fish Canyon Tuff (Fig. 19c and d). We infer that these homogeneous areas (hereafter 'glass') approximate liquid compositions, even though they almost certainly have undergone post-emplacement hydration.

Glasses in both Pagosa Peak Dacite and outflow Fish Canyon Tuff are high-SiO_2 rhyolite (76·5–78 wt % SiO_2, Table 7) with high K_2O (5·2–5·8 wt %), and correspondingly low CaO (0·6–0·8 wt %), FeO_{tot} (0·3–0·8 wt %) and MgO (<0·1 wt %, close to detection limit). Na content is also relatively low (2·1–3·2 wt %) in comparison with other rhyolites (3–4 wt %: Bishop Tuff, Anderson *et al.*, 2000; Glass Mountain lavas, Metz & Mahood, 1991). Some Na loss during secondary hydration could be in part responsible for these low values, although the sums of the oxides of the analyses are high for hydrated glasses (97–98%) and Na/K ratios do not vary widely. The colorless Pagosa Peak Dacite glass and the glass in the outflow Fish Canyon Tuff vitrophyres span the same range of composition as the homogeneous

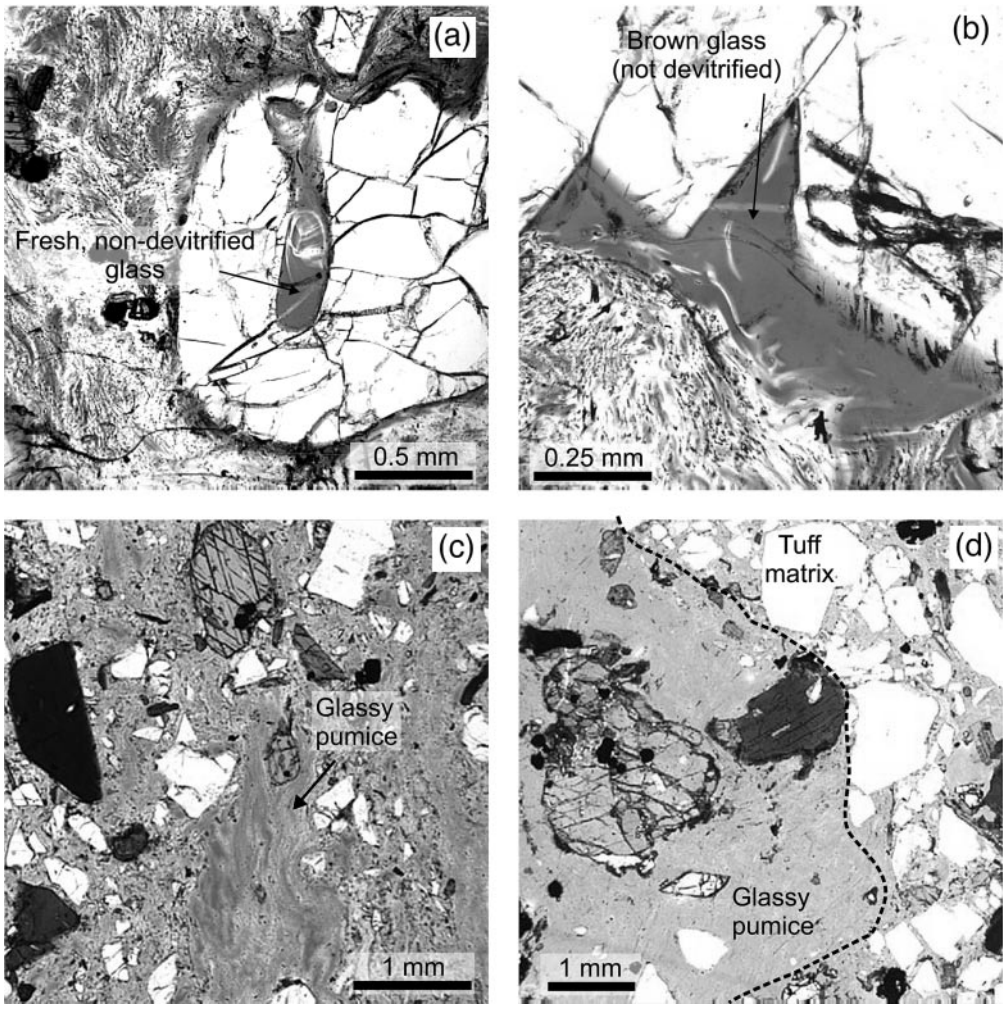

Fig. 19. Interstitial glass in Fish Canyon magma (all images in plane-polarized light). (a) and (b) are both from Pagosa Peak Dacite magmatic blobs (Bfc 83). Although the matrix remains glassy, the formation of minute oxide filaments during incipient devitrification has rendered the glass around it colorless (iron loss). However, in areas bordering phenocrysts and in large melt pools inside remelted crystals, glass remained free of even the oxide filaments and has retained its brown coloration. Microprobe analyses in these zones are inferred to provide reliable compositions of the Fish Canyon melt immediately before eruption. (c) Small glassy pumices in an outflow Fish Canyon Tuff vitrophyre (Bfc 113). (d) Glassy pumice from an intracaldera Fish Canyon Tuff vitrophyre (Bfc 191a).

brown glass in Pagosa Peak Dacite, except for lower Fe in the colorless glass. Glass in pumices of one intracaldera Fish Canyon Tuff sample is slightly lower in SiO_2 (76–77 wt %) and higher in K_2O and TiO_2 (Bfc 191, Table 7). The four glass analyses reported by Whitney & Stormer (1985, table 6) and the matrix analysis reported by Johnson & Rutherford (1989*a*, table 1) have slightly lower CaO and Al_2O_3 contents with correspondingly higher K_2O and Na_2O.

Our analyses of non-devitrified natural glasses in multiple units of the Fish Canyon system are close in composition to the experimentally produced melt in equilibrium with the Fish Canyon mineral assemblage at $X_{H_2O} = 0{\cdot}5$, 2 kbar, andradite–magnetite–quartz–hedenbergite (AMQH) f_{O_2} buffer, and 760°C (Johnson & Rutherford, 1989*a*). Both of these liquids contain minor An component (normative Ab/An = 5–8) and the modest shift of the position of the minimum melt toward the Qz–Or join, relative to experimental glasses in the haplogranitic Qz–Ab–Or ternary, is consistent with experimental results taking into account the role of Ca (e.g. Johannes & Holtz, 1996). Johnson & Rutherford (1989*a*) argued that the activity of H_2O was well below unity in this system, as plagioclase in water-saturated Fish Canyon magma at this temperature is far more An rich than the observed compositions. The relatively low activity of H_2O in the Fish Canyon magma can be partly explained by the presence of S (Fish Canyon magma contains pyrrhotite; Whitney & Stormer, 1983, 1985; Parat, 2001) and halogens (up to 1·5 wt % F in biotite, and 2·5–3 wt % F in apatite).

Table 7: Average major element glass compositions from the Fish Canyon magma

	PPD (n = 28)	FCT (O) (n = 69)	FCT (I) (n = 255)	Xtal-rich PPD (n = 9)	Xtal-rich FCT (I) (n = 7)
SiO_2	77·55±0·74	77·66±0·43	76·75±0·45	77·29±0·56	77·28±0·70
TiO_2	0·15±0·03	0·13±0·02	0·24±0·05	0·13±0·01	0·13±0·01
Al_2O_3	12·74±0·14	12·63±0·13	12·53±0·18	12·96±0·06	13·23±0·05
FeO_{tot}	0·55±0·22	0·66±0·97	0·60±0·16	0·69±0·13	0·66±0·08
MnO	0·06±0·03	0·04±0·03	0·04±0·03	0·07±0·04	0·03±0·03
MgO	0·06±0·02	0·06±0·02	0·07±0·02	0·07±0·01	0·07±0·02
CaO	0·72±0·05	0·72±0·05	0·72±0·07	0·74±0·03	0·56±0·02
Na_2O	2·70±0·25	2·79±0·15	2·79±0·22	2·82±0·16	3·60±0·09
K_2O	5·39±0·21	5·50±0·13	6·10±0·25	5·18±0·14	4·41±0·23
P_2O_5	0·01±0·01	0·02±0·02	0·02±0·03	0·01±0·01	0·01±0·01
Na_2O/K_2O	0·50±0·06	0·50±0·03	0·46±0·06	0·55±0·04	0·82±0·06

All analyses normalized to 100% anhydrous.

To assess the origin of the interstitial liquid in the Fish Canyon magma, trace elements compatible with the main mineral phases found in the magma were analyzed and compared with other high-SiO_2 rhyolites. Sr and Ba have high partition coefficients for plagioclase and sanidine, respectively. The model of Blundy & Wood (1991) yields a partition coefficient of ~20 for Sr in An_{30} plagioclase at 760°C, and the Ba partition coefficient in K-feldspar (Or_{70}) is thought to exceed 10 (Nash & Crecraft, 1985; Icenhower & London, 1996). In magmas where the mineral assemblage is feldspar rich, such as in the Fish Canyon magma, Sr and Ba contents in the interstitial melt should differ markedly, depending on whether feldspars are crystallizing or melting. Liquids (glass) produced by melting are predicted to have high Sr and Ba contents (Tomassini & Davies, 1997). In contrast, fractional crystallization should produce residual melts strongly depleted in these elements (Halliday *et al.*, 1991). High-SiO_2 rhyolites such as the Glass Mountain lavas (Halliday *et al.*, 1989; Metz & Mahood, 1991), the Bishop Tuff (Anderson *et al.*, 2000), and the Bandelier Tuff (Dunbar & Hervig, 1992), in which fractional crystallization is thought to have played a major role, have low Sr (0·1–5 ppm) and Ba (1–80 ppm) contents. Conversely, granitoid xenoliths from Tatara–San Pedro (Costa, 2000) and Crater Lake (Bacon, 1992), which partially remelted during residence in their host magmas, have interstitial glass with concentrations of Sr and Ba up to 50 times higher than the Bishop, Bandelier, and Glass Mountain samples. The Fish Canyon interstitial glass (60–90 ppm Sr, and 480–560 ppm Ba) belongs to the high Sr–Ba group, suggesting that it is not residual from extreme feldspar fractionation, in agreement with textural observations.

In contrast, other trace elements, such as Y, HREE, and Zr, reach low concentrations in the Fish Canyon glass (i.e. Y 5–6 ppm, Yb <1 ppm, Zr ~70 ppm) and ratios of La/Yb and Rb/Y are unusually high (~35–40) for a high-SiO_2 rhyolite. By comparison, Glass Mountain lavas have La/Yb and Rb/Y ratios of 6–10 (Metz & Mahood, 1991). These significant depletions in Y, HREE, and Zr relative to the whole-rock composition suggest partitioning into hornblende and accessory phases, such as sphene and zircon, again consistent with the euhedral morphologies of these phases in the Fish Canyon magma.

In summary, all major, minor and trace elements compatible in the euhedral phenocrysts phases (biotite, hornblende and accessory phases) in Fish Canyon magma are highly depleted in the interstitial glass, whereas elements compatible in feldspars are enriched in comparison with other high-SiO_2 rhyolites. These diverse enrichments and depletions of trace elements in glass can be explained in a general sense in accord with other observations: (1) crystallization of hornblende, biotite, and accessory phases; (2) resorption of feldspars. We note, however, that the high concentrations of Ba and Sr are even more remarkable in light of the observation of some regrowth of both plagioclase (reversely zoned euhedral rims) and sanidine (Rapakivi-textured overgrowths) that must have incorporated both these elements (particularly Ba in sanidine). Were it not for feldspar regrowth, the Sr and Ba excesses over the concentrations in Glass Mountain, Bishop Tuff and Bandelier Tuff glasses would have been even larger. Based on a single laser-ablation inductively coupled plasma mass spectrometry (ICP-MS) analysis of the Fish Canyon interstitial glass (191, Table 8), the Eu content of the glass appears to be consistent with this interpretation, as it is ~10 times higher (0·32 ppm) than

Table 8: Ion probe analyses of Fish Canyon hornblende and glass

	59hb3p-2 Hbl (PPD)	59hb3-1 Hbl (PPD)	59hb3-2 Hbl (PPD)	191 Gl (FCTI)	59MT-1 Gl (PPD)	59MT-2 Gl (PPD)	59MT-3 Gl (PPD)
SiO_2	47	47	47	74	76	76	76
CaO	11·6	11·8	11·8	0·6	0·5	0·6	0·5
K_2O	0·8	0·8	0·7	5·9	5·3	5·3	5·3
TiO_2	1·3	1·2	1·2	0·2	0·1	0·1	0·1
Li	4·6	5·2	5·2	58·3	28·3	29·3	50·3
Rb	15·6	16·6	14·4	288·4	227·9	225·3	214·8
Sr	38·3	40·3	37·8	84·9	60·2	58·4	93·6
Y	83·9	73·8	84·2	6·4	6·2	5·2	5·6
Zr	50·0	45·0	49·1	79·4	71·1	70·9	70·3
Nb	37·4	30·3	35·3	19·7	13·1	12·5	12·4
Ba	23·7	32·1	30·8	477·5	542·0	503·0	562·0
La	58·0	52·9	56·1	33·1	36·5	32·8	33·2
Ce	175	154	169	54	49	43	43
Pr	24·4	21·4	23·2	—	3·4	2·9	2·8
Nd	99·6	95·1	102·0	9·4	9·5	7·8	7·9
Sm	19·0	17·9	21·1	1·3	1·1	1·0	0·9
Eu	3·3	3·3	3·5	0·3	Interf.	Interf.	Interf.
Gd	15·1	14·3	14·2	4·1	Interf.	Interf.	Interf.
Tb	3·0	3·0	3·1	—	0·2	0·1	0·1
Dy	17·2	15·3	16·7	0·9	0·8	0·5	0·8
Ho	3·2	3·1	3·4	—	0·3	0·2	0·2
Er	9·8	9·1	10·8	0·6	0·6	0·8	0·6
Yb	11·7	9·9	11·4	1·0	0·9	1·0	0·8

Ion microprobe analyses were performed at the University of Edinburgh, with the assistance of R. Hinton, using a Cameca IMS-4f ion microprobe with an O-primary beam of net impact energy of 15 keV and an operating current of 5–8 nA. Beam diameter ranged between 15 and 30 μm. The concentrations were obtained by normalizations of mass ^{30}Si to the silica values obtained by electron microprobe analyses. The SRM-610 glass standard was used to monitor day-to-day changes in experimental conditions. The ion yields relative to SRM-610 were calculated using Lake County plagioclase for plagioclase, SHF1 alkali feldspar for sanidine, and Corning glass for the glass. Hornblende ion yields were close enough to the standard to avoid correction (R. Hinton, personal communication, 1997). The 2σ precision for most elements is <5% relative. Error of >10% relative can occur only in La, Ce, Y and Rb. The glass analysis from the FCT (I) was performed in Lausanne using laser ablation ICP-MS (François Bussy analyst). SiO_2, CaO, K_2O, and TiO_2 in wt % oxide, the rest in ppm.

in Glass Mountain Lavas (Metz & Mahood, 1991) and melt inclusions in quartz of the Bishop Tuff (Anderson *et al.*, 2000), but it is comparable with concentrations measured in partially melted xenoliths from Crater Lake (Bacon, 1992) and Tatara–San Pedro (Costa, 2000).

MAGMATIC INCLUSIONS

Previously unrecognized characteristics of the Fish Canyon magmatic system are the occurrence of (1) holocrystalline granodioritic xenoliths with the same mineralogy and similar whole-rock compositions and mineral chemistry as Fish Canyon magma, and (2) hybrid andesite inclusions (Pl + Kfs + Hbl + Cpx + Mag + matrix). These two types of inclusions, found up to now only in the late-erupted intracaldera tuff, provide useful information about the origin and the evolution of the Fish Canyon magma.

Holocrystalline granodioritic xenoliths

Rare (≪0·1%) fragments of holocrystalline granodiorite, 5–30 cm in diameter, are present in the late-erupted upper intracaldera Fish Canyon Tuff on the northern slopes of the resurgent dome, as well as in the post-Fish Canyon Huerto Andesite (F. Parat, personal communication, 2001). The granodiorites show no evidence of deformation, have the same mineral assemblage as

Fish Canyon magma (Pl + Kfs + Qtz + Hbl + Bt + Spn + Mag + Ilm + Ap + Zrn; Fig. 20a), and have similar modal abundances of hydrous phases (Hbl and Bt), sphene, and oxides. The modal differences reside in the higher proportions of quartz, K-feldspar, and plagioclase in the granodiorites, reflecting the absence of glass in these samples. They are coarse grained (0·5–5 mm), with individual crystals similar in size to Fish Canyon phenocrysts. Hornblende, biotite, plagioclase, and sphene are generally euhedral, whereas K-feldspar and quartz are interstitial and anhedral (Fig. 20a). Some K-feldspar grains, like large sanidine crystals in Fish Canyon magma, contain numerous isolated, anhedral plagioclase inclusions in optical continuity included within Ba-rich zones, suggesting replacement of plagioclase by K-feldspar and development of Rapakivi textures. Some of these xenoliths also contain interstitial granophyre.

The whole-rock compositions of the granodioritic xenoliths (~67·2 wt % SiO_2) are close to the Fish Canyon magma composition. With the exception of Mn and Ca, relative differences in major and minor elements concentration are <10%. Among trace elements, Nd, Pb, Cr, and Zn are different by >50%, but all the others are within 15% of the Fish Canyon value (Table 2). Likewise, mineral compositions span similar ranges, although subtle variations are present. Concentrations of all major elements in hornblendes and biotites from the granodiorite xenoliths largely overlap those of the Fish Canyon Tuff (Fig. 21). The linear trends defined in variation diagrams by the Fish Canyon Tuff hornblendes are slightly extended by the xenolith data toward lower Al_2O_3 (<5 wt % Al_2O_3), and correspondingly lower FeO_{tot} and higher MgO and SiO_2, consistent with crystallization at even lower temperatures than those recorded in the Fish Canyon hornblendes. Similarly, biotites in xenoliths have, on average, slightly higher SiO_2, and lower FeO and TiO_2. Average K-feldspar compositions in the granodiorites are shifted toward lower K (~Or_{68} instead of Or_{72}) content, whereas plagioclase is slightly more albitic (to ~An_{20}). The more albitic compositions are largely restricted to the outermost rims of plagioclase. A microprobe traverse across a large plagioclase from a granodiorite yielded a core composition typical of Fish Canyon plagioclase (~An_{30}), overgrown by a normally zoned rim of ~200 μm thickness falling to An_{20}.

The similarities in mineralogy, texture, whole-rock composition and mineral chemistry displayed by the granodioritic fragments and the Fish Canyon magma suggests that they are relics of a plutonic facies of the Fish Canyon magma chamber. These xenoliths may be the products of a prolonged early history involving multiple stages of magma emplacement, during which early Rapakivi textures were produced, or they may have solidified immediately before eruption at the same time as the formation of decompression-related granophyric overgrowths on sanidine crystals in the Fish Canyon magma. Similar granodioritic xenoliths found in the Huerto Andesite imply that holocrystalline Fish Canyon material was still present in the crust after the caldera-forming eruption.

Hybrid andesitic inclusions

Hybrid andesitic inclusions are rare, occurring only in the upper intracaldera Fish Canyon Tuff. They are fist-sized reddish enclaves with fine-grained textures and have sharp boundaries with the host tuff (Fig. 20c). The mineral assemblage is hornblende, sanidine, plagioclase, clinopyroxene, and oxides in a microlite-rich devitrified matrix (Fig. 20d). Hornblende and sanidine reach 1 mm in diameter, whereas the other phases range in size from 50 to 500 μm. The mafic minerals (hornblende and clinopyroxene) have reaction rims. Sanidine phenocrysts and plagioclase microlites are euhedral, and sanidine is commonly poikilitic.

The absence of biotite in combination with the presence of clinopyroxene, the more calcic compositions of plagioclase microlites ($An_{60–40}$), and the andesitic whole-rock composition indicate that these inclusions originated from more mafic magma that was injected into or entrained by Fish Canyon magma. A hybrid origin is inferred from (1) the presence of euhedral, poikilitic sanidines in the relatively mafic inclusions, suggesting some mixing with K-rich melt, and (2) zones rich in Fish Canyon minerals (Fig. 20c). In response to their incorporation in the hotter, more mafic liquid, the scavenged Fish Canyon phenocrysts have been corroded, and Fish Canyon plagioclase grains have euhedral overgrowths (50–100 μm thick) with more calcic compositions ($An_{37–40}$). Such textures are typical following the entrainment of plagioclase phenocrysts in a more mafic magma (i.e. Larsen *et al.*, 1938; Feeley & Dungan, 1996). The mingled mafic inclusions show that the Fish Canyon magma interacted with a more mafic counterpart while both were still partly liquid.

A MULTISTAGE MODEL FOR THE ORIGIN OF THE FISH CANYON MAGMA: REJUVENATION OF A SHALLOW, PARTIALLY SOLIDIFIED BATHOLITH BY MAGMATIC UNDERPLATING

The Fish Canyon magma displays a rich catalog of textural and chemical information, from which its late magmatic evolution can be deduced. We have stressed

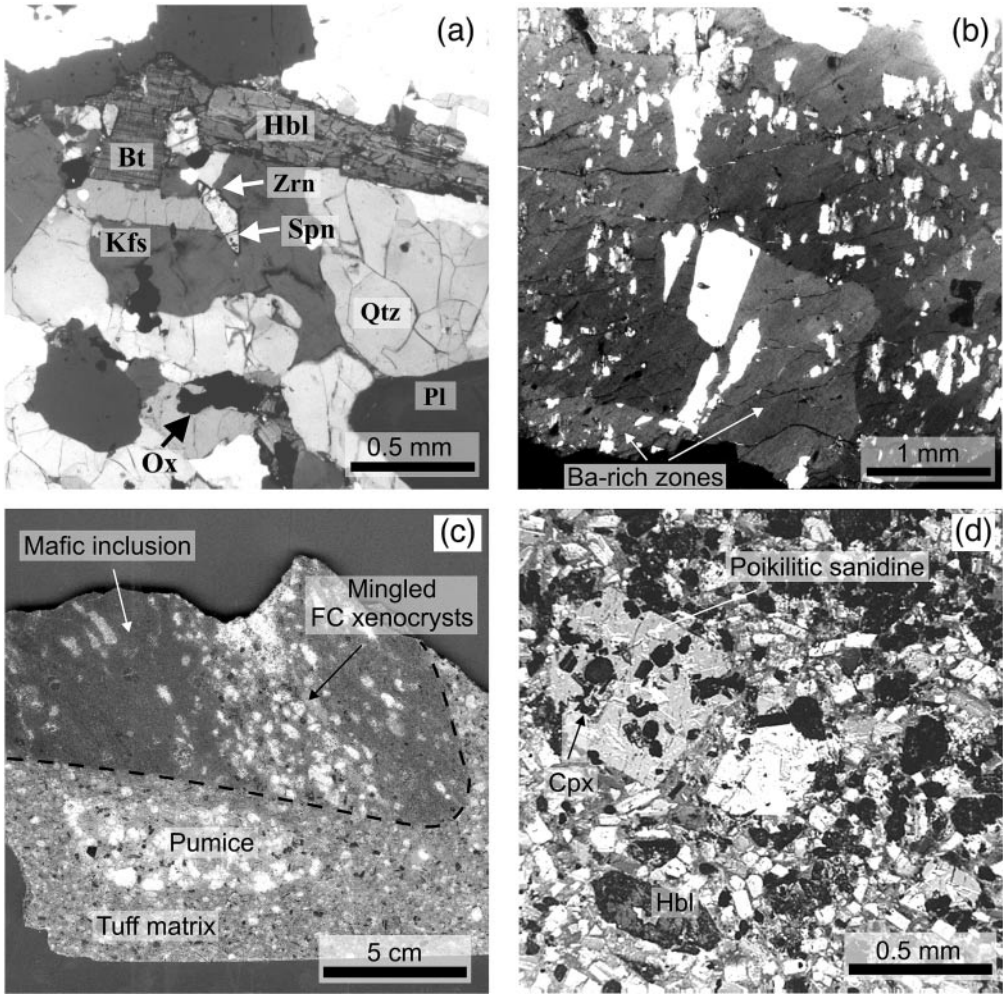

Fig. 20. Photomicrographs of granodioritic fragments and hybrid andesite inclusions entrained in the intracaldera Fish Canyon Tuff. (a) Fish Canyon mineral assemblage in a granodioritic xenolith (Bfc 187; partially crossed polars). Mineral compositions in this granodiorite overlap extensively with those in Fish Canyon magma (Fig. 21). (b) Large poikilitic K-feldspar, containing plagioclase inclusions in optical continuity and Ba-rich zones (Bfc 187; crossed polars) (c) Macroscopic view of a hybrid andesite inclusion enclosed in the intracaldera Fish Canyon Tuff, showing a band of mingled crystal-rich Fish Canyon magma marked by a high concentration of xenocrysts (MLX QMI). (d) The only occurrence of pyroxene and euhedral sanidine in the Fish Canyon magmatic system, which are both present in the andesitic inclusions. The clinopyroxenes are also found free in the matrix of the inclusions and, like hornblendes, always show oxidized rims (QMI 2; plane-polarized light). The fine-grained texture should be noted, showing K-rich sanidine (Or_{72-80}) and plagioclase microlites more calcic than average Fish Canyon plagioclases (An_{40-60} instead of An_{27-33}).

the importance of resorption textures in quartz, sanidine, and plagioclase phenocrysts (Figs 10 and 17) and the production of some anatectic high-SiO_2 rhyolite melt just before eruption, but we have also documented that the ferromagnesian phases were crystallizing during the latter stages of magma evolution (Fig. 6), and that sanidine and plagioclase are characterized by resorption textures in some grains and late crystallization in others (Figs 10, 11 and 13). The development of Rapakivi-like textures (Figs 12, 13, 14 and 16), reverse compositional zoning and 'calcic spikes' in plagioclase phenocryst rims (Fig. 11), reverse Al_2O_3 zoning in hornblende (Fig. 9), and multistage coupled diffusion profiles across sanidine–plagioclase grain boundaries (Fig. 18) are evidence for thermal perturbations tied to a dominant up-temperature trend in the Fish Canyon magma chamber shortly before eruption, probably in conjunction with some mass addition (mainly H_2O-rich fluids?). Completely solid xenoliths with Fish Canyon bulk composition, mineralogy, and mineral chemistry indicate that parts of this system were completely solid, but the absence of evidence for dehydration melting coupled with mass- and thermal-balance considerations indicate that the rejuvenated portion of the system retained a small fraction of water-rich interstitial melt. Mineral barometry and thermometry on natural and experimental samples of

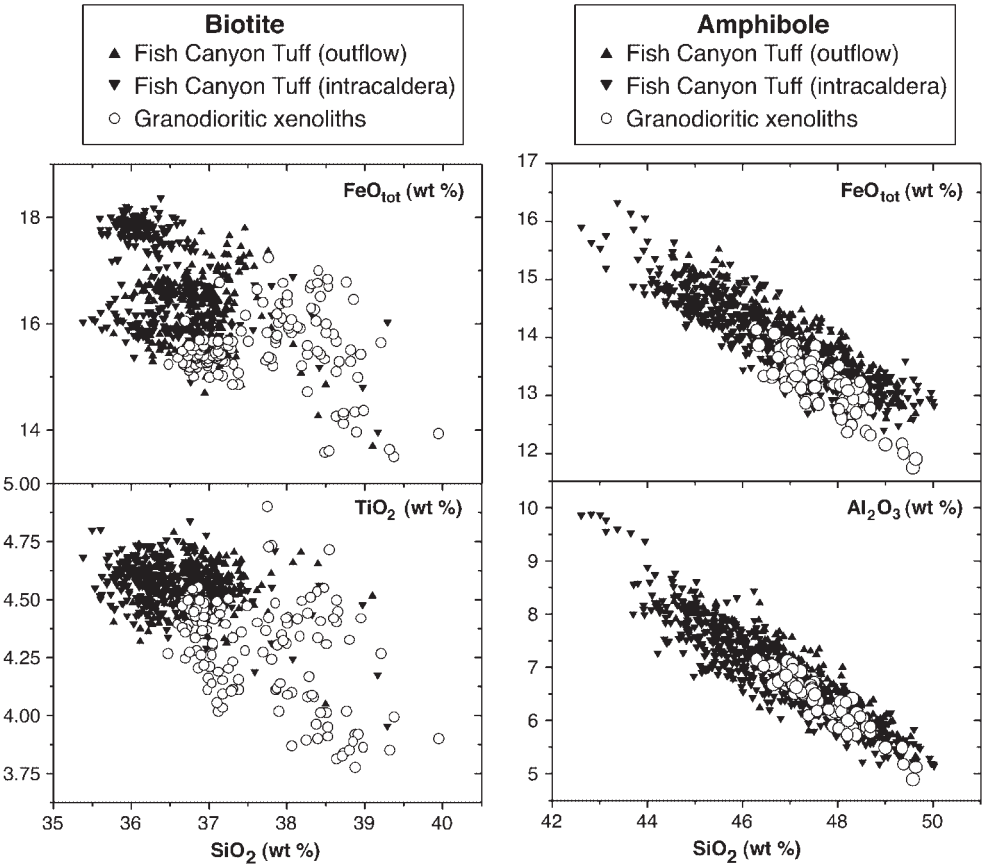

Fig. 21. Major element variation diagrams comparing analyses of hornblende and biotite in Fish Canyon magma (intracaldera and outflow Fish Canyon Tuff) with the same phases in the granodioritic xenoliths. In terms of hornblende composition, fields do not perfectly overlap, but are largely similar, whereas biotite compositions in the granodioritic xenoliths are slightly shifted towards lower FeO_{tot} and TiO_2.

the Fish Canyon magma (Johnson & Rutherford, 1989*a*; Bachmann & Dungan, 2002) are consistent with a shallow depth of magma residence, in accord with eruption from a caldera, and with a temperature ~70–100°C above the water-saturated granodioritic solidus. Integration of these textural and chemical observations with experimental results on the Fish Canyon magma and similar silicic systems leads to a multistage model for the origin and evolution of the Fish Canyon magma (Fig. 22) in which: (1) >5000 km^3 of dacitic magma were emplaced in the upper crust: (2) this magma partially solidified to form a conductively cooling crystal mush; (3) underplating of more mafic volatile-rich magma resulted in rejuvenation via new melt production, convective remobilization, and finally eruption of this magma.

Although the model that we propose for the overall origin and evolution of the Fish Canyon magmatic system requires the sequential operation of multiple processes, there are currently inadequate constraints on whether original magma genesis, emplacement of this magma in the upper crust, partial solidification (either by decompression of wet magma and/or by cooling), and subsequent rejuvenation following influx of mantle-derived magma occurred as a continuum or as multiple short-lived events separated widely in time from the others. As the system as a whole is so large, it is probable that both the initial emplacement of the protolith batholith and the later intrusive events responsible for its rejuvenation were incremental. Consequently, we suspect that the textural complexity observed in Fish Canyon magma originated in a system that experienced many mass additions and thermal fluctuations both during initial shallow accumulation of magma and subsequently during the pre-eruptive up-temperature stage.

This paper focuses on the late evolution of the Fish Canyon magma, but the origin of the 'parental' magma is an important issue that we are currently addressing. In regions such as long-lived convergent continental margins, where the crust is characterized by elevated thermal gradients related to long-term injection of mantle-derived magma (5–6 Myr in the case of the Central San Juan volcanic field), partial melting of the crust is a predictable consequence and it is considered to be the primary mechanism responsible for generation of

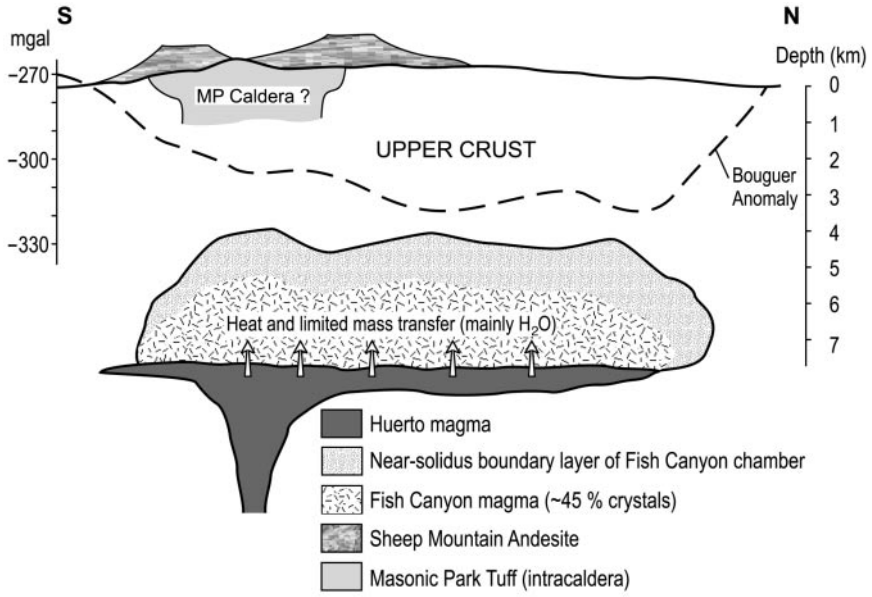

Fig. 22. Schematic cross-section of the upper crust in the central San Juan region just before onset of the Fish Canyon volcanism. Vertical exaggeration = 5 (horizontal extent of the chamber is close to 100 km). Thicknesses of the different magmatic components are highly speculative, and are constrained mainly by the overall volume estimate of erupted magma, the area of the La Garita caldera, its barometric estimates from Fish Canyon hornblende, and the experimental results of Johnson & Rutherford (1989*a*). Asymmetry of Huerto intrusion with its feeder in the south is based on field observations such as the focus of Huerto volcanism around the southern margin of the La Garita caldera [see text and Lipman (2000) for details] and on the shape of the Bouguer gravity anomaly (Plouff & Pakiser, 1972 It should be stressed that the negative Bouguer gravity anomaly is, however, a representation of the present-day structure of the crust, and extrapolation to the time of the Fish Canyon cycle should be undertaken with caution. MP caldera, Masonic Park caldera, which formed ~600 kyr before the onset of Fish Canyon eruptions.

granitoid batholiths. As a general rule, the isotopic compositions of evolved magmas erupted from the Central San Juan caldera cluster are consistent with subequal proportions of crustal and mantle components (Lipman *et al.*, 1978; Riciputi *et al.*, 1995), if the basaltic component did not originate in isotopically evolved lithospheric mantle. If mantle-derived magmas were characterized by $\varepsilon_{Ndi} > 1$, typical andesitic to dacitic eruptive products of the San Juan volcanic field ($\varepsilon_{Ndi} = -5$ to -8) either must be the products of open-system differentiation involving substantial assimilation, or they were generated by partial melting of crust that had been previously hybridized by injections of mantle-derived magma. Both processes probably played important roles in San Juan magmatism, but the enormous volume of Fish Canyon magma, and the presence of Precambrian zircons (Lanphere & Baadsgaard, 2001), lead us to favor partial melting of hybridized Proterozoic crust, in accord with the close resemblance of the Fish Canyon magma to average batholithic granodiorite (Fig. 5; Nockolds *et al.*, 1978).

Basaltic magmatism is well established as the main heat carrier in volcanically active areas (e.g. Hildreth, 1981; Bergantz & Dawes, 1994), and interactions between the Fish Canyon magma and more mafic components are indicated, despite limited physical mixing. Rare hybrid mafic enclaves are present in the upper part of the intracaldera Fish Canyon Tuff, which is inferred to represent the deepest part of the magma chamber. Some of the mafic magma likely to have been responsible for the rejuvenation and remobilization of the Fish Canyon magma body apparently reached the surface. The Huerto Andesite (Lipman, 1975, 2000; Askren *et al.*, 1991), which directly overlies the Fish Canyon Tuff, consists of ~200 km^3 of andesitic lavas and breccias exposed mainly in and around the southern La Garita caldera. Parat (2001) has estimated temperatures of ~800–900°C for water-rich hornblende + anhydrite + pyrrhotite-bearing andesites erupted from centers located near the southern margin of the La Garita caldera. Thus, a close temporal–spatial association between the Fish Canyon magma and a substantial quantity of volatile-rich andesitic magma is reasonably well established.

If the Fish Canyon magma was rejuvenated immediately before eruption, it is important to ascertain whether or not this magma body attained complete solidification before reheating. The presence of holocrystalline comagmatic xenoliths indicates that some parts of the magma chamber crystallized completely, but these do not require that the whole chamber was ever entirely solidified. The widespread occurrence of multiphase aggregates with solid–solid grain contacts in Fish Canyon magma, in combination with remelting textures displayed by feldspars and quartz, plus high Ba–Sr glass

compositions with a compositional signature inherited from melting of feldspars, suggest that the whole magma batch reached a higher crystallinity than was recorded at eruption, but other evidence seems to require that interstitial liquid never completely disappeared. Water is essential for melting in the upper crust at temperatures below 800°C. The dry solidus for the haplogranitic system is close to 1000°C at 2 kbar, whereas it falls to ~680°C under water-saturated conditions (Johannes & Holtz, 1996). If the protolith had been completely solidified, the breakdown of hydrous phases to anhydrous minerals (dehydration melting) would have been needed to provide water, at least in the early stages (Clemens & Vielzeuf, 1987; Bergantz & Dawes, 1994). The textural evidence against hornblende and biotite breakdown, and the absence of pyroxene in Fish Canyon magma make it highly unlikely that dehydration melting occurred during the rejuvenation process and suggest instead that water-rich interstitial liquid was always present.

The water budget of the Fish Canyon magma also supports the inference that magma solidification did not reach completion on a chamber-wide scale. Totally solidified Fish Canyon magma, represented by the granodioritic xenoliths, would contain substantially less than 1 wt % H_2O, assuming 5–8 vol. % each of hornblende and biotite with ~2 and ~3 wt % H_2O, respectively. If the erupted magma had completely crystallized at any stage, a large volume of water, corresponding to 2·5–3 wt % H_2O in the final magma body, must have been transferred during reheating from the underlying crystallizing mafic magma to account for the inferred presence of 3–3·5 wt % dissolved water immediately before eruption (Johnson & Rutherford, 1989*a*). If the subjacent hornblende-bearing Huerto andesitic magmas contained a minimum of ~2–4 wt % H_2O (Askren *et al.*, 1991; Parat, 2001), a volume of mafic to intermediate magma comparable with that of the Fish Canyon magma would be required to supply enough water, even if H_2O were transferred with perfect efficiency from the underlying mafic reservoir. It is unlikely that the amount of Huerto magma was coequal to that of the Fish Canyon magma, and the presence of hornblende-rich cumulate gabbroic xenoliths (~50 modal % amphibole) in Huerto Andesite at Eagle Mountain (Parat, 2001) suggests that a substantial fraction of the available H_2O was retained in Huerto magma reservoirs. Thus, the externally derived quantity of H_2O that would be required for partial remelting of a completely frozen Fish Canyon pluton is unrealistically large.

None the less, there are a few petrologic observations suggesting that fluid transfer from the underlying magma did occur, and this process may have contributed to remelting by lowering the solidus temperature of the Fish Canyon crystal mush and decreasing the viscosity and density of interstitial melt, thereby enhancing convective motions. Relatively high Cl in some apatite crystals in interstitial glass (~1 wt % Cl, twice as much as in the Bishop Tuff apatites; Whitney & Stormer, 1985; F. Parat, personal communication, 2001), the stability of hornblende and biotite during reheating, and marked increases in fluorine in the rims of some biotite phenocrysts (independent of variations in Fe/Mg_{Biot}) all point to fluid additions. Whether these fluxes occurred entirely through diffusion across the mafic–silicic interface (Litvinovsky & Podladchikov, 1993; Bindeman & Davis, 1999), or by the ascent and mixing of an H_2O-rich fluid phase is currently unresolved.

The residence time of the Fish Canyon magma in the shallow crust before rejuvenation is not constrained precisely. We think it likely that initial partial solidification was related to decompression of wet magma (Cashman & Blundy, 2000; Blundy & Cashman, 2001). However, a recent analytical treatment of the thermal evolution of large igneous bodies (Koyaguchi & Kaneko, 1999) suggests that near-solidus magma chambers are capable of remaining in the upper crust for long periods of time as crystal mushes. If one assumes that solidification is driven largely by cooling, an initial phase dominated by convective loss of heat runs its course relatively rapidly, but once the magma body becomes too crystalline to convect, conduction prevails and cooling rates decrease dramatically. Residence times in the range of 10^5 years are inferred for conductively cooling crystal mush bodies (Koyaguchi & Kaneko, 1999). A period spanning 1×10^5 to 5×10^5 years for this exceptionally large system would be consistent with currently available geochronological constraints on early central San Juan caldera-related volcanism (Lipman, 2000).

Alternative models

Alternative end-member models for the generation of 5000 km^3 of homogeneous crystal-rich dacitic Fish Canyon magma are: (1) single-stage differentiation from a more mafic parental magma accompanied by extremely efficient segregation of dacitic magma from the refractory residue; or (2) single-stage partial melting of the deep crust without a period of shallow residence and partial solidification. Progressive evolution of mafic magma (± crustal contributions) is commonly cited as a process responsible for generating ash-flow tuff magmas, particularly those that display compositional and thermal gradients [however, see Eichelberger *et al.* (2000)]. Single-stage differentiation of mafic magma is an unlikely mechanism for 5000 km^3 of Fish Canyon magma, which is one of the least compositionally heterogeneous large pyroclastic units. As the fraction of dacitic magma (~68 wt % SiO_2) that could be derived by differentiation of primitive basalt is ~0·1–0·2, the volume of basalt

parental to the Fish Canyon magma would be ~25 000–50 000 km^3, or ~60–125% of the estimated erupted volume of the long-lived San Juan volcanic field. Thus, on the basis of volumetric arguments alone, this scenario appears to be untenable. Open-system magma generation, involving substantial assimilation of crust by a large mass of intermediate magma intruded in the upper crust (e.g. Riciputi *et al.*, 1995), might serve to replicate the conditions and textures observed in the Fish Canyon magma, but is plagued by the same aforementioned mass- and thermal-balance considerations. The second possibility resembles the magma generation and rapid ascent model proposed by Whitney & Stormer (1985). As the experimental studies of Johnson & Rutherford (1989*a*, 1989*b*) and our re-evaluation of the pressure implications of Fish Canyon minerals and coexisting melt discredit previously cited evidence for preservation of a high-pressure stage of magma residence, there is no longer any direct support for this model.

Magma dynamics and mass balance during rejuvenation

Despite its enormous volume and the inferred presence of a hot mafic intrusion beneath it, the Fish Canyon magma chamber was remarkably homogeneous immediately before eruption in terms of modal abundances, whole-rock chemistry, mineral chemistry (this paper), and oxygen isotopes in quartz, magnetite and zircon (I. N. Bindeman, unpublished data, 2001). The degree to which homogenization was achieved during the rejuvenation stage is difficult to gauge because the scale and magnitude of heterogeneity before late-stage heating is undetermined. Many batholithic intrusions with comparable volumes are comparably homogeneous. However, all samples are characterized by a combination of mineral growth and mineral resorption plus a variety of mineral zoning profiles. The conjunction of homogeneity at the scale of this enormous magma chamber with extreme textural complexity at the millimeter to centimeter scale implies a highly dynamic system, in which parcels of magma with different thermal histories were mixed during convective or advective transport.

Broadly similar scenarios for magma rejuvenation following renewed mafic input into long-lived upper-crustal magmatic systems have been proposed as the origin of volumetrically small quantities (<5 km^3) of intermediate to silicic magma associated with large calderas (Wolff & Gardner, 1995) and active arc volcanoes (Matthews *et al.*, 1999; Murphy *et al.*, 2000), ignimbrites of significant volume (Keller, 1970; Mahood, 1990), as well as for silicic plutons (Wiebe, 1994; Wiebe *et al.*, 1997; Robinson & Miller, 1999). The example that most closely resembles the Fish Canyon case in terms of textural complexity and mineral disequilibrium is the 1995–present andesitic eruption of the Soufrière Hills on Montserrat (Murphy *et al.*, 2000; Couch *et al.*, 2001). On the basis of this continuing eruptive episode, wherein multiple historic injections of basalt are inferred from seismic swarms and surface manifestations, Couch *et al.* (2001) have proposed that a pre-existing crystal-rich mush heated from below has undergone convective self-mixing as the thin thermal boundary layer at the contact with the mafic magma became buoyant and rose as plumes into the overlying colder interior. Such a mechanism, which may be extrapolated to much more voluminous systems, provides the necessary means to bring relatively cool, crystal-rich descending plumes from the roof of the system into direct contact with hotter ascending crystal-poor plumes into which solid phases could be dissolved.

This latter point is critical in that magma rejuvenation in the Fish Canyon system occurred mainly through remelting of quartz and feldspar to produce a highly 'evolved' pseudo-eutectic melt. In contrast, reverse compositional trends combined with oscillatory growth zoning in euhedral plagioclase and hornblende, and large F variations across euhedral biotite phenocrysts, imply that these minerals were growing as other phases were melting. Alternating regrowth and dissolution of K-feldspar and plagioclase are recorded by the Ba-rich growth zones on the peripheries of some sanidine phenocrysts in association with discontinuous Rapakivi-like plagioclase mantles on sanidine during periods of K-feldspar dissolution. A finger-like convection regime is a plausible mechanism for creating and assembling these diverse crystalline manifestations of magma rejuvenation. This dynamic regime allows crystals with contrasting thermal histories that originated in different parts of the system to be located in close proximity in the final magma chamber configuration. The coupling of concurrent resorption and growth may in fact be a useful criterion for identifying rejuvenated magmas, as it has been described in other systems that apparently followed similar up-temperature evolution paths (Matthews *et al.*, 1999; Murphy *et al.*, 2000; Couch *et al.*, 2001).

Although the modal increases in hornblende and biotite during up-temperature evolution of the magma were small (a few modal percent), this counter-intuitive aspect of the Fish Canyon system can be explained if the prevalent interstitial high-SiO_2 rhyolite melt were mixed with buoyant, water-rich melts containing higher normative proportions of anorthite and ferromagnesian components. As the Fish Canyon high-SiO_2 rhyolite matrix liquid consisted almost entirely of network-forming components, and coexistence with 11 solid phases was maintained throughout the system, such a liquid might have behaved as a transfer medium from which network-modifying components were precipitated almost as rapidly as they were added from below. Mass additions may

have been supplied either as highly evolved differentiation products liberated by the underlying volatile-rich magma body or by bulk melting of Fish Canyon crystal mush near the contact with the mafic magma. These mechanisms are more likely than direct injection of a hot mafic magma, as we see almost no evidence of quenched magmatic inclusions or the crystalline debris that typically results from their disaggregation and dispersion.

The dynamic scenario proposed here, which is based closely on the model of Couch *et al.* (2001), provides an internally consistent explanation for the seemingly contradictory observations that minerals were simultaneously growing and dissolving and that the fraction of melt in the Fish Canyon magmatic system increased immediately before eruption. Whether or not the same mode of genesis applies universally to the class of voluminous ignimbrites classed by Hildreth (1981) as Monotonous Intermediates remains to seen, but many of these units have the same general characteristics as the Soufrière Hills and Fish Canyon magmas (e.g. Francis *et al.*, 1989; Lindsay *et al.*, 2001).

ACKNOWLEDGEMENTS

The help of G. F. Marriner and M. F. Thirlwall [X-ray fluorescence (XRF) spectroscopy; University of London at Royal Holloway and Bedford New College], N. Rogers [instrumental neutron activation analysis (INAA); Open University), R. Hinton (ion microprobe; University of Edinburgh), I. Bindeman (oxygen isotopes; University of Wisconsin), F. Bussy (electron microprobe; University of Lausanne), F. Capponi (XRF; University of Geneva), J.-M. Boccard (thin-section preparation; University of Geneva) and J. Metzger (computer-aided drawing; University of Geneva) was greatly appreciated. We are grateful for generous hospitality and logistical support provided by Ren Thompson during past and current field studies in the San Juan volcanic field. This work benefited from numerous discussions with colleagues from the University of Geneva and other institutions. Special thanks go to Bernard Evans, who first suggested that the complex Fish Canyon sanidines could be analogous to Rapakivi textures. Our thinking about the mechanics of the model we propose has benefited immensely from numerous discussions with George Bergantz and Steve Sparks. Costs of fieldwork were supported by the USGS Volunteer Program and by Swiss FNRS grant 20-49730.96, which also provided funding for laboratory analyses. Malcom Rutherford, Shan de Silva, and Calvin Miller are thanked for detailed and constructive reviews of the manuscript, and we are grateful to Gareth Davies for the editorial effort invested in this paper.

REFERENCES

Ague, J. J. (1997). Thermodynamic calculation of emplacement pressures for batholithic rocks, California; implications for the aluminum-in-hornblende barometer. *Geology* **25**(6), 563–566.

Anderson, A. T., Davis, A. M. & Lu, F. (2000). Evolution of the Bishop Tuff rhyolitic magma based on melt and magnetite inclusions and zoned phenocrysts. *Journal of Petrology* **41**(3), 449–473.

Anderson, J. L. (1996). Status of thermobarometry in granitic batholiths. *Transactions of the Royal Society of Edinburgh: Earth Sciences* **87**, 125–138.

Anderson, J. L. & Smith, D. R. (1995). The effects of temperature and f_{O2} on the Al-in-hornblende barometer. *American Mineralogist* **80**, 549–559.

Askren, R. R., Whitney, J. A. & Roden, M. F. (1991). Petrology and geochemistry of the Huerto Andesite, San Juan volcanic field, Colorado. *Contributions to Mineralogy and Petrology* **107**, 373–386.

Bachmann, O. & Dungan, M. A. (2002). Temperature-induced aluminium zoning in hornblendes of the Fish Canyon magma, Colorado. *American Mineralogist* (submitted).

Bachmann, O., Dungan, M. A. & Lipman, P. W. (2000). Voluminous lava-like precursor to a major ash-flow tuff: low-column pyroclastic eruption of the Pagosa Peak Dacite, San Juan volcanic field, Colorado. *Journal of Volcanology and Geothermal Research* **98**, 153–171.

Backlund, H. G. (1938). The problems of the rapakivi granites. *Journal of Geology* **46**, 339–396.

Bacon, C. R. (1992). Partially melted granodiorite and related rocks ejected from Crater Lake caldera, Oregon. *Transactions of the Royal Society of Edinburgh: Earth Sciences* **83**, 27–47.

Bergantz, G. W. & Dawes, R. (1994). Aspects of magma generation and ascent in continental lithosphere. In: Ryan, M. P. (ed.) *Magmatic Systems*. San Diego, CA: Academic Press, pp. 291–317.

Best, M. G. & Christiansen, E. H. (1997). Origin of broken crystals in ash-flow tuffs. *Geological Society of America Bulletin* **109**, 63–73.

Bindeman, I. N. & Davis, A. M. (1999). Convection and redistribution of alkalis and trace elements during the mingling of basaltic and rhyolitic melts. *Petrology* **7**(1), 91–101.

Blundy, J. & Cashman, K. (2001). Ascent-driven crystallisation of dacite magmas at Mount St Helens, 1980–1986. *Contributions to Mineralogy and Petrology* **140**, 631–650.

Blundy, J. D. & Holland, T. J. B. (1990). Calcic amphibole equilibria and a new amphibole–plagioclase geothermometer. *Contributions to Mineralogy and Petrology* **104**(2), 208–224.

Blundy, J. D. & Wood, B. J. (1991). Crystal-chemical control on the partitioning of Sr and Ba between plagioclase feldspar, silicate melts, and hydrothermal solutions. *Geochimica et Cosmochimica Acta* **55**, 193–209.

Brown, S. J. A. & Fletcher, I. R. (1999). SHRIMP U–Pb dating of the preeruption growth history of zircons from the 340 ka Whakamaru Ignimbrite, New Zealand: Evidence for >250 k.y. magma residence times. *Geology* **27**(1), 1035–1038.

Cashman, K. & Blundy, J. (2000). Degassing and crystallization of ascending andesite and dacite. *Philosophical Transactions of the Royal Society of London, Series A* **358**, 1487–1513.

Clemens, J. D. & Vielzeuf, D. (1987). Constraints on melting and magma production in the crust. *Earth and Planetary Science Letters* **86**, 287–306.

Colucci, M. T., Dungan, M. A. & Fergusson, K. M. (1991). Precaldera lavas of the southeast San Juan volcanic field: parent magmas and crustal interactions. *Journal of Geophysical Research* **96**(B8), 13413–13434.

Costa, F. (2000). The petrology and geochemistry of diverse crustal xenoliths, Tatara–San Pedro Volcanic Complex, Chilean Andes. Ph.D. thesis, University of Geneva.

Couch, S., Sparks, R. S. J. & Carroll, M. R. (2001). Mineral disequilibrium in lavas explained by convective self-mixing in open magma chambers. *Nature* **411**, 1037–1039.

Czamanske, G. K. & Wones, D. R. (1973). Oxidation during magmatic differentiation, Finnmarka Complex, Oslo area, Norway: Part 2, the mafic silicates. *Journal of Petrology* **14**(3), 349–381.

Davis, J. M., Elston, W. E. & Hawkesworth, C. J. (1993). Basic and intermediate volcanism of the Mogollon–Datil volcanic field: implications for mid-Tertiary tectonic transitions in southwestern New Mexico, USA. In: Prichard, H. M., Alabaster, T., Harris, N. B. W. & Neary, C. R. (eds) *Magmatic Processes and Plate Tectonics. Geological Society, London, Special Publications* **76**, 469–488.

de Silva, S. L. (1991). Styles of zoning in the central Andean ignimbrites: insights into magma chamber processes. In: Harmon, R. S. & Rapela, C. W. (eds) *Andean Magmatism and its Tectonic Setting. Geological Society of America, Special Paper* **265**, 233–243.

Dunbar, N. W. & Hervig, R. L. (1992). Volatile and trace element composition of melt inclusions from the lower Bandelier Tuff: implications for magma chamber processes and eruptive style. *Journal of Geophysical Research* **97**(B11), 15151–15170.

Eichelberger, J. C., Chertkoff, D. G., Dreher, S. T. & Nye, C. J. (2000). Magmas in collision; rethinking chemical zonation in silicic magmas. *Geology* **28**(7), 603–606.

Elkins, L. T. & Grove, T. L. (1990). Ternary feldspar experiments and thermodynamic models. *American Mineralogist* **75**, 544–559.

Feeley, T. C. & Dungan, M. A. (1996). Compositional and dynamic controls on mafic–silicic magma interactions at continental arc volcanoes: evidence from Cordòn El Guadal, Tatara–San Pedro Complex, Chile. *Journal of Petrology* **37**(6), 1547–1577.

Francis, P. W., Sparks, R. S. J., Hawkesworth, C. J., Thorpe, R. S., Pyle, D. M., Tait, S. R., Mantovani, M. S. & McDermott, F. (1989). Petrology and geochemistry of the Cerro Galan caldera, northwest Argentina. *Geological Magazine* **126**(5), 515–547.

Gardner, A. & McPhie, J. (1999). Partially melted lithic megablocks in the Yardea Dacite, Gawler Range Volcanics, Australia: implications for eruption and emplacement mechanisms. *Bulletin of Volcanology* **61**, 396–410.

Grove, T. L., Kinzler, R. J., Baker, M. B., Donnelly-Nolan, J. M. & Lesher, C. E. (1988). Assimilation of granite by basaltic magma at Burnt Lava flow, Medicine Lake volcano, northern California: decoupling of heat and mass transfer. *Contributions to Mineralogy and Petrology* **99**, 320–343.

Grunder, A. L. & Boden, D. R. (1987). Comment on '... magmatic conditions of the Fish Canyon Tuff, central San Juan volcanic field, Colorado' by Whitney & Stormer (1985). *Journal of Petrology* **28**, 737–746.

Halliday, A. N. (1990). Reply to comment of R. S. J. Sparks, H. E. Huppert, and C. J. N. Wilson on 'Evidence for long residence times of rhyolitic magma in the Long Valley magmatic system: the isotopic record in precaldera lavas of Glass Mountain'. *Earth and Planetary Science Letters* **99**, 390–394.

Halliday, A. N., Mahood, G. A., Holden, P., Metz, J. M., Dempster, T. J. & Davidson, J. P. (1989). Evidence for long residence times of rhyolitic magma in the Long Valley magmatic system: the isotopic record in precaldera lavas of Glass Mountain. *Earth and Planetary Science Letters* **94**, 274–290.

Halliday, A. N., Davidson, J. P., Hildreth, W. & Holden, P. (1991). Modeling the petrogenesis of high Rb/Sr silicic magmas. *Chemical Geology* **92**, 107–114.

Hammarstrom, J. M. & Zen, E.-a. (1986). Aluminium in hornblende: an empirical igneous geobarometer. *American Mineralogist* **71**, 1297–1313.

Hildreth, W. (1981). Gradients in silicic magma chambers: implications for lithospheric magmatism. *Journal of Geophysical Research* **86**(B11), 10153–10192.

Holland, T. & Blundy, J. (1994). Non-ideal interactions in calcic amphiboles and their bearing on amphibole–plagioclase thermometry. *Contributions to Mineralogy and Petrology* **116**, 433–447.

Hollister, L. S., Grissom, G. C., Peters, E. K., Stowell, H. H. & Sisson, V. B. (1987). Confirmation of the empirical correlation of Al in hornblende with pressure of solidification of calc-alkaline plutons. *American Mineralogist* **72**, 231–239.

Housh, T. B. & Luhr, J. F. (1991). Plagioclase–melt equilibria in hydrous systems. *American Mineralogist* **76**, 477–492.

Icenhower, J. & London, D. (1996). Experimental partitioning of Rb, Cs, Sr, and Ba between alkali feldspar and peraluminous melt. *American Mineralogist* **81**, 719–734.

Johannes, W. & Holtz, F. (1996). *Petrogenesis and Experimental Petrology of Granitic Rocks*. Berlin: Springer, 335 pp.

Johnson, M. & Rutherford, M. (1989a). Experimentally determined conditions in the Fish Canyon Tuff, Colorado, magma chamber. *Journal of Petrology* **30**, 711–737.

Johnson, M. C. & Rutherford, M. J. (1989b). Experimental calibration of the aluminum-in-hornblende geobarometer with application to Long Valley Caldera (California) volcanic rocks. *Geology* **17**, 837–841.

Kaczor, S. M., Hanson, G. N. & Peterman, Z. E. (1988). Disequilibrium melting of granite at the contact with basic plug: a geochemical and petrographic study. *Journal of Geology* **96**, 61–78.

Keller, J. (1970). Origin of rhyolites by anatectic melting of granitic crustal rocks; the example of rhyolitic pumice from the island of Kos (Aegean Sea). *Bulletin of Volcanology* **33**(3), 942–959.

Koyaguchi, T. & Kaneko, K. (1999). A two-stage thermal evolution model of magmas in continental crust. *Journal of Petrology* **40**(2), 241–254.

Lanphere, M. A. & Baadsgaard, H. (2001). Precise K–Ar, $^{40}Ar/^{39}Ar$, Rb–Sr, U/Pb mineral ages from the 27·5 Ma Fish Canyon Tuff reference standard. *Chemical Geology* **175**, 653–671.

Larsen, E. S., Jr, Irving, J., Gonyer, F. A. & Larsen, E. S. (1936–1938). Petrologic results of a study of the minerals from the Tertiary volcanic rocks of the San Juan region, Colorado. *American Mineralogist* **21**, 666–701; **22**, 889–905; **23**, 227–257, 417–429.

Lindsay, J. M., Schmitt, A. K., Trumbull, R. B., De Silva, S. L., Siebel, W. & Emmermann, R. (2001). Magmatic evolution of the La Pacana caldera system, Central Andes, Chile: compositional variation of two cogenetic, large-volume felsic ignimbrites. *Journal of Petrology* **42**(3), 459–486.

Lipman, P. W. (1975). *Evolution of the Platoro Caldera Complex and Related Volcanic Rocks, Southeastern San Juan Mountains, Colorado. US Geological Survey, Professional Paper* **852**, 128 pp.

Lipman, P. W. (2000). The central San Juan caldera cluster: regional volcanic framework. In: Bethke, P. M. & Hay, R. L. (eds) *Ancient Lake Creede: its Volcano-Tectonic Setting, History of Sedimentation, and Relation of Mineralization in the Creede Mining District. Geological Society of America, Special Paper* **346**, 9–69.

Lipman, P. W., Steven, T. A. & Mehnert, H. H. (1970). Volcanic history of the San Juan mountains, Colorado, as indicated by potassium–argon dating. *Geological Society of America Bulletin* **81**, 2329–2351.

Lipman, P. W., Protska, H. J. & Christiansen, R. L. (1972). Cenozoic volcanism and plate-tectonic evolution of western United States, I, Early and middle Cenozoic. *Philosophical Transactions of the Royal Society of London, Series A* **271**, 217–248.

Lipman, P. W., Doe, B. & Hedge, C. (1978). Petrologic evolution of the San Juan volcanic field, Southwestern Colorado: Pb and Sr isotope evidence. *Geological Society of America Bulletin* **89**, 59–82.

Lipman, P. W., Dungan, M. A., Brown, L. L. & Deino, A. L. (1996). Recurrent eruption and subsidence at the Platoro Caldera complex,

southeastern San Juan volcanic field, Colorado; new tales from old tuffs. *Geological Society of America Bulletin* **108**, 1039–1055.

Lipman, P. W., Dungan, M. A. & Bachmann, O. (1997). Comagmatic granophyric granite in the Fish Canyon Tuff, Colorado: implications for magma-chamber processes during a large ash-flow eruption. *Geology* **25**(10), 915–918.

Litvinovsky, B. A. & Podladchikov, Y. Y. (1993). Crustal anatexis during the influx of mantle volatiles. *Lithos* **30**(2), 93–107.

Lowenstern, J. B., Clynne, M. A. & Bullen, T. D. (1997). Comagmatic A-type granophyre and rhyolite from the Alid volcanic center, Eritrea, Northeast Africa. *Journal of Petrology* **38**(2), 1707–1721.

Mahood, G. A. (1990). Second reply to comment of R. S. J. Sparks, H. E. Huppert, and C. J. N. Wilson on 'Evidence for long residence times of rhyolitic magma in the Long Valley magmatic system: the isotopic record in precaldera lavas of Glass Mountain'. *Earth and Planetary Science Letters* **99**, 395–399.

Matthews, S. J., Sparks, R. S. J. & Gardeweg, M. C. (1999). The Piedras Grandes–Soncor eruptions, Lascar volcano, Chile; evolution of a zoned magma chamber in the central Andean upper crust. *Journal of Petrology* **40**(2), 1891–1919.

Metz, J. M. & Mahood, G. A. (1991). Development of the Long Valley, California, magma chamber recorded in precaldera rhyolite lavas of Glass Mountain. *Contributions to Mineralogy and Petrology* **106**, 379–397.

Munoz, J. L. (1984). F–OH and Cl–OH exchange in micas with applications to hydrothermal ore deposits. In: Bailey, S. W. (ed.) *Micas. Mineralogical Society of America, Reviews in Mineralogy* **13**, 469–493.

Murphy, M. D., Sparks, R. S. J., Barclay, J., Carroll, M. R. & Brewer, T. S. (2000). Remobilization of andesitic magma by intrusion of mafic magma at the Soufrière Hills Volcano, Montserrat, West Indies. *Journal of Petrology* **41**(1), 21–42.

Nash, W. P. & Crecraft, H. R. (1985). Partition coefficients for trace elements in silicic magmas. *Geochimica et Cosmochimica Acta* **49**, 2309–2322.

Nockolds, S. R., Knox, R. W. & Chinner, G. A. (1978). *Petrology for Students*. Cambridge: Cambridge University Press, 435 pp.

Parat, F. (2001). Contemporaneous magmatic differentiation of S-rich trachyandesite and high-K calc-alkaline andesite in an intra-continental setting, San Juan volcanic field, Colorado, U.S.A. Ph.D. thesis, University of Geneva.

Plouff, D. & Pakiser, L. C. (1972). Gravity study in the San Juan Mountains, Colorado. *US Geological Survey, Professional Paper* **800**, B183–B190.

Reid, M. R. & Coath, C. D. (2000). *In situ* U–Pb ages of zircons from the Bishop Tuff: no evidence for long crystal residence times. *Geology* **28**(5), 443–446.

Reid, M. R., Coath, C. D., Harrison, T. M. & McKeegan, K. D. (1997). Prolonged residence times for the youngest rhyolites associated with Long Valley Caldera: ^{230}Th–^{238}U microprobe dating of young zircons. *Earth and Planetary Science Letters* **150**, 27–39.

Riciputi, L. R., Johnson, C. M., Sawyer, D. A. & Lipman, P. W. (1995). Crustal and magmatic evolution in a large multicyclic caldera complex: isotopic evidence from the central San Juan volcanic field. *Journal of Volcanology and Geothermal Research* **67**, 1–28.

Robinson, D. M. & Miller, C. F. (1999). Record of magma chamber processes preserved in accessory mineral assemblages, Aztec Wash pluton, Nevada. *American Mineralogist* **84**, 1346–1353.

Rutherford, M. J. & Devine, J. D. (1988). The May 18, 1980, eruption of Mount St. Helens: 3. Stability and chemistry of amphibole in the magma chamber. *Journal of Geophysical Research* **93**, 11949–11959.

Scaillet, B. & Evans, B. W. (1999). The 15 June 1991 eruption of Mount Pinatubo. I. Phase equilibria and pre-eruption P–T–fO$_2$–fH$_2$O conditions of the dacite magma. *Journal of Petrology* **40**(3), 381–411.

Schmidt, M. W. (1992). Amphibole composition in tonalite as a function of pressure; an experimental calibration of the Al-in-hornblende barometer. *Contributions to Mineralogy and Petrology* **110**(2–3), 304–310.

Sederholm, J. J. (1891). Über die finnländischen Rapakivigesteine. *Tschermak's Mineralogische und Petrographische Mitteilungen* **12**, 1–31.

Smith, J. V. (1974). *Feldspar Minerals: Chemical and Textural Properties*. Berlin: Springer.

Sparks, R. S. J., Huppert, H. E. & Wilson, C. J. N. (1990). Comment on 'Evidence for long residence times of rhyolitic magma in the Long Valley magmatic system: the isotopic record in precaldera lavas of Glass Mountain' by A. N. Halliday, G. A. Mahood, P. Holden, J. M. Metz, T. J. Dempster, J. P. Davidson. *Earth and Planetary Science Letters* **99**, 387–389.

Spear, F. S. (1981). An experimental study of hornblende stability and compositional variability in amphibolite. *American Journal of Science* **281**, 697–734.

Steven, T. A. (1975). Mid-Tertiary volcanic field in the southern Rocky Mountains. *Geological Society of America, Memoir* **144**, 75–94.

Steven, T. A. & Lipman, P. W. (1976). Calderas of the San Juan volcanic field, southwestern Colorado. *US Geological Survey, Professional Paper* **958**, 1–35.

Stimac, J. A. & Wark, D. A. (1992). Plagioclase mantles on sanidine in silicic lavas, Clear Lake, California; implications for the origin of rapakivi texture. *Geological Society of America Bulletin* **104**(6), 728–744.

Stormer, J. C., Jr & Whitney, J. A. (1985). Two feldspar and iron–titanium oxide equilibria in silicic magmas and the depth of origin of large volume ash-flow tuffs. *American Mineralogist* **70**, 52–64.

Sun, S., S. & McDonough, W. F. (1989). Chemical and isotopic systematics of oceanic basalts: implications for mantle composition and processes. In: Saunders, A. D. & Norry, M. J. (eds) *Magmatism in the Ocean Basins. Geological Society, London, Special Publications* **42**, 313–345.

Taylor, S. R. & McLennan, S. M. (1985). *The Continental Crust: its Composition and Evolution*. Oxford: Blackwell.

Tomassini, S. & Davies, G. R. (1997). Isotope disequilibrium during anatexis: a case study of contact melting, Sierra Nevada, California. *Earth and Planetary Science Letters* **148**, 273–285.

Tuttle, O. F. & Bowen, N. L. (1958). *Origin of Granite in Light of Experimental Studies in the System $NaAlSi_3O_8$–$KAlSi_3O_8$–SiO_2. Geological Society of America, Memoir* **74**, 153 pp.

van den Bogaard, P. & Schirnick, C. (1995). ^{40}Ar/^{39}Ar laser probe ages of Bishop Tuff quartz phenocrysts substantiate long-lived silicic magma chamber at Long Valley, United States. *Geology* **23**(8), 759–762.

Vorma, A. (1971). Alkali feldspars of the Wiborg Massif in southeastern Finland. *Bulletin de la Commission Géologique de Finlande* **246**, 1–72.

Vyhnal, C. R., McSween, H. Y. & Speer, J. A. (1991). Hornblende chemistry in southern Appalachian granitoids: implications for aluminium hornblende thermobarometry and magmatic epidote stability. *American Mineralogist* **76**, 176–188.

Wahl, W. (1925). Die Gesteine des Wiborger Rapakiwigebietes. *Fennia* **45**(0), 1–127.

Wark, D. A. & Stimac, J. A. (1992). Origin and mantled (rapakivi) feldspars; experimental evidence of a dissolution- and diffusion-controlled mechanism. *Contributions to Mineralogy and Petrology* **111**(3), 345–361.

Watson, E. B. (1982). Basalt contamination by continental crust: some experiments and models. *Contributions to Mineralogy and Petrology* **56**, 73–87.

Wen, S. & Nekvasil, H. (1994). SOLVCALC; an interactive graphics program package for calculating the ternary feldspar solvus and for two-feldspar geothermometry. *Computers and Geosciences* **20**(6) 1025–1040.

Whitney, J. A. & Stormer, J. C. (1983). Igneous sulfides in the Fish Canyon Tuff and the role of sulfur in calc-alkaline magmas. *Geology* **11**, 99–102.

Whitney, J. A. & Stormer, J. C., Jr (1985). Mineralogy, petrology, and magmatic conditions from the Fish Canyon Tuff, central San Juan volcanic field, Colorado. *Journal of Petrology* **26**, 726–762.

Wiebe, R. A. (1994). Silicic magma chambers as traps for basaltic magmas: the Cadillac Mountain intrusive complex, Mount Desert Island, Maine. *Journal of Geology* **102**, 423–437.

Wiebe, R. A., Smith, D., Sturm, M., King, E. M. & Seckler, M. S. (1997). Enclaves in the Cadillac Mountain granite (coastal Maine): samples of hybrid magma from the base of the chamber. *Journal of Petrology* **38**(3), 393–423.

Wolff, J. A. & Gardner, J. N. (1995). Is the Valles Caldera entering a new cycle of activity? *Geology* **23**(5), 411–414.